Using information content to determine the sensitivity of AIRS channels to mid-latitude ice clouds in single- and multi-layer regimes

Ashtin Massie

A Thesis submitted in partial fulfillment of

the requirements for the degree of

Master of Science

(Atmospheric and Oceanic Sciences)

at the

University of Wisconsin-Madison

August 2019

Thesis Declaration and Approval

I, Ashtin Massie, declare that this Thesis titled 'Using information content to determine the sensitivity of AIRS channels to mid-latitude ice clouds in single- and multi-layer regimes' and the work presented in it are my own.

Ashtin Massie		
Author	Signature	Date

I hereby approve and recommend for acceptance this work in partial fulfillment of the requirements for the degree of Master of Science:

Tristan L'Ecuyer		
Committee Chair	Signature	Date

Grant Petty		
Faculty Member	Signature	Date

Elisabeth Weisz		
Associate Scientist	Signature	Date

Abstract

Using information content to determine the sensitivity of AIRS channels to mid-latitude ice clouds in single- and multi-layer regimes

by Ashtin Massie

From increasing the planetary albedo to decreasing the Earth's outgoing longwave radiation, clouds have a significant influence on the Earth's energy budget and climate. However, clouds and aerosols continue to contribute the largest uncertainty to our understanding of the Earth's response to global climate change (Boucher et al. 2013). A large portion of this uncertainty is because of ice clouds, whose properties satellites can have difficulty retrieving and thus can be underrepresented in cloud datasets used to inform climate models. In single-layer cases, the thin nature of upper-level ice clouds makes retrievals problematic; in multi-layer cases, which have an estimated annual mean occurrence near 30% (L'Ecuyer et al., 2019), the reflection and emission from lower level clouds influence the radiation field observed by satellites, muddling the retrieval of the separate cloud layers and posing a challenge for both conventional observations and models. Due to the different challenges in retrieving single-layer and multi-layer ice clouds, treating these cases separately can improve retrieval algorithms and enhance global cloud datasets. This study will focus on assessing the information content of satellite hyperspectral radiances for ice clouds in single- and multi-layer regimes. Using an ensemble of ice cloud regimes derived from the Atmospheric Radiation Measurement (ARM) Southern Great Plains site from 2003-2009, and modeling the radiances that would be measured by the Atmospheric

Infrared Sounder (AIRS) when these ice clouds are present, we are able to narrow down the AIRS channels that are the most sensitive to the properties of certain mid-latitude ice clouds and see how the sensitivity of these channels changes in scenes with multiple cloud layers. We found that in single-layer cases, longwave channels near 9.5 μm, 11 μm, and 13 μm were preferentially selected as containing the most information about ice clouds. While some of these longwave channels remained important in the multi-layer scenes, the information of shortwave channels between 3.8 and 4.2 μm increased substantially with the introduction of low-level clouds. This selection of channels and their significance will be explored more thoroughly throughout this paper.

Acknowledgements

Here, I would like to say thank you to Tristan L'Ecuyer, Elisabeth Weisz, Grant Petty, and the L'Ecuyer Group for providing feedback, support, and guidance throughout this process. I would also like to thank my family and friends for their continual encouragement, support, and positivity.

Contents

List of Figures

Abbreviations

AIRS	**A**tmospheric **I**nfra**R**ed **S**ounder
ARM	**A**tmospheric **R**adiation **M**easurement
CCN	**C**loud **C**ondensation **N**uclei
CPR	**C**loud **P**rofiling **R**adar
CRE	**C**loud **R**adiative **E**ffect
CrIS	**Cr**oss-track **I**nfrared **S**ounder
IASI	**I**nfrared **A**tmospheric **S**ounding **I**nterferometer
LTE	**L**ocalized **T**hermodynamic **E**quilibrium
NeDT	**N**oise **E**quivalent **T**emperature **D**ifference
SGP	**S**outhern **G**reat **P**lains
TOA	**T**op **O**f **A**tmosphere
WMO	**W**orld **M**eteorological **O**rganization
CTT	**C**loud **T**op **T**emperature
$\mathbf{D_e}$	Effective **D**iameter
IWC/(LWC)	**I**ce (**L**iquid) **W**ater **C**ontent
IWP/(LWP)	**I**ce (**L**iquid) **W**ater **P**ath
K	**K**elvin
hPa	**H**ectopascal
μ**m**	Micrometer
τ	Optical depth

Chapter 1

Introduction

Clouds have varying but significant influences on the Earth's energy budget and climate, and understanding their processes is essential to our ability to create accurate climate models. However, clouds and aerosols continue to contribute the largest uncertainty to our understanding of the Earth's changing energy balance in response to global climate change (Boucher et al. 2013). Specifically, the manner in which ice clouds contribute to climate change remains particularly complex. In single layers, ice clouds tend to have a warming effect on the atmosphere; however, their occurrence in multi-layer cloud scenes, which tends to occur more frequently than single-layer scenes globally, changes the net radiative effects of upper-level ice clouds from warming to cooling (L'Ecuyer et al., 2019). These contrasting effects indicate that the radiative effects of ice clouds are highly sensitive to the presence or absence of underlying cloud layers, which complicates the contribution of ice clouds to the Earth's radiative budget. The response of these different

types of ice clouds to climate change can be equally complicated, as our ability to model changes of global ice cloud coverage and multi-layer cloud scenes depends on our ability to observe various cloud regimes in the present and then effectively use those observations to parameterize the cloud processes of these scenes in climate models. However, the optically thin nature of these ice clouds makes them difficult to monitor and model, and their occurrence in multi-layer cloud scenes complicates satellite retrievals, as underlying low-level cloud layers can dramatically alter our ability to accurately retrieve upper-level cloud properties through reflection and absorption processes. Thus, improving the detection of ice clouds and their properties from space-borne instruments in single- and multi-layer regimes is essential, both for improving our understanding of the global cloud radiative effects of ice clouds and for reducing the overall uncertainty associated with clouds in climate models.

This study will focus on improving the retrieval of ice cloud properties in the mid-latitudes using the high-spectral-resolution Atmospheric Infrared Sounder (AIRS). The AIRS instrument (https://airs.jpl.nasa.gov), launched in 2002 onboard NASA's Aqua satellite, contains 2378 spectral channels in the infrared spectrum and can be used to retrieve the properties of clouds on a global scale at a relatively high horizontal and vertical resolution. More specifics about the AIRS instrument will be described in this paper. Here, we look to use an information content analysis to determine the optimal set of AIRS channels for the retrieval of the properties of ice clouds observed in the mid-latitudes, in both single-layer and multi-layer cloud scenes. We explore the impact that the presence of low-level clouds has on the selection of AIRS channels that contain

the most information about upper-level ice clouds, with the goal of contributing to the advancement of ice cloud retrievals across a multitude of settings.

1.1 Clouds and the Earth's Radiative Budget

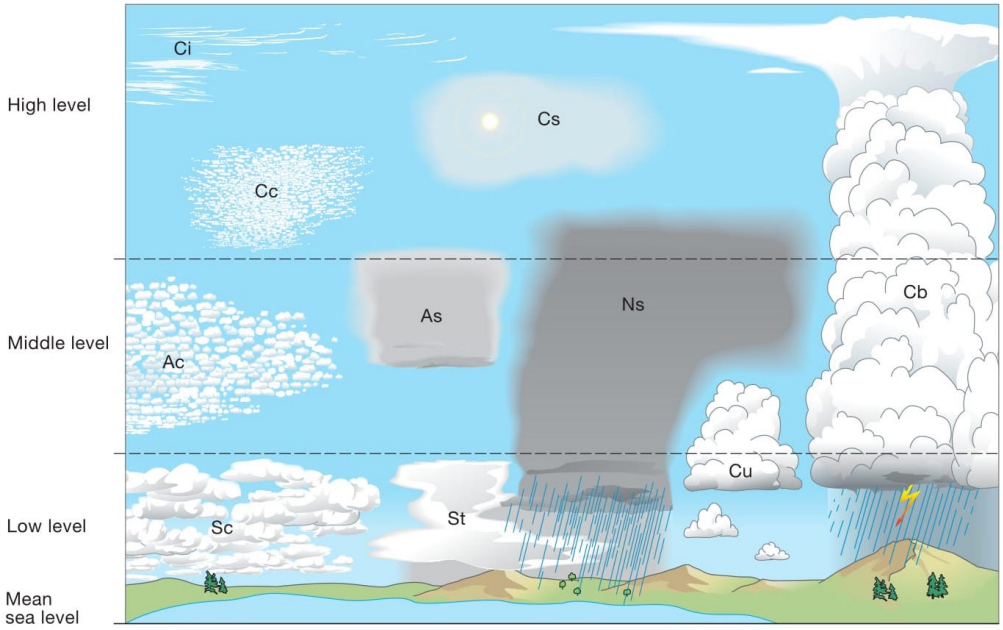

FIGURE 1.1: The 10 cloud genera within their allocated level or levels as classified by the World Meteorological Organization (2017).

On average, clouds cover nearly 70% of the globe (Stubenrauch et al., 2013). While the cloud fraction depends on the detection sensitivity and the spatial resolution of cloud profiling instruments (Wielicki and Parker, 1992), nevertheless we can say that clouds are an intrinsic component of the atmosphere year-round. Globally, around 40–50 percent of clouds observed are classified as high clouds, with cloud top pressures below 440 hectopascals (hPa); about 15 percent are classified as mid-level clouds with no higher clouds

above them, with cloud top pressures between 440 and 680 hPa; and 40 percent are classified as single-layer low clouds, with cloud top pressures above 680 hPa (Stubenrauch et al., 2013). These broad cloud classifications can be broken down further to account for varying optical, radiative, or microphysical properties. The World Meteorological Organization (WMO) breaks down the clouds at these three levels into 10 genera of clouds, shown in Figure 1.1 and Figure 1.2 (World Meteorological Organization, 2017). While most clouds stick to the levels in which they are classified, the thicker cloud types, such as cumulus (Cu), nimbostratus (Ns), altostratus (As), and cumulonimbus (Cb), can extend to various levels. Thus, defining specific cloud boundaries is essential for classification and analysis.

Level	*Genera*	*Polar region*	*Temperate region*	*Tropical region*
High	Cirrus Cirrocumulus Cirrostratus	3 – 8 km (10 000 – 25 000 ft)	5 – 13 km (16 500 – 45 000 ft)	6 –18 km (20 000 – 60 000 ft)
Middle	Altocumulus Altostratus Nimbostratus	2 – 4km (6 500 – 13 000 ft)	2 – 7 km (6 500 – 23 000 ft)	2 – 8 km (6 500 – 25 000 ft)
Low	Stratus Stratocumulus Cumulus Cumulonimbus	From the Earth's surface to 2 km (0 – 6 500ft)	From the Earth's surface to 2 km (0 – 6 500ft)	From the Earth's surface to 2 km (0 – 6 500ft)

FIGURE 1.2: Approximate heights of each cloud level, and the genera occurring in each (World Meteorological Organization, 2017).

High-level clouds are typically composed of ice crystals of various geometries, and are typically found in the upper troposphere, with their cloud top pressure below 440 hPa and their base generally at least 5 kilometers above the surface, although this altitude varies depending on the depth of the troposphere (World Meteorological Organization,

2017). Generally, pure ice clouds occur at temperatures below -40°C; temperatures above this can contain liquid or supercooled liquid cloud drops. The general ice cloud classification includes cirrus (Ci), cirrostratus (Cs), and cirrocumulus (Cc). In general, cirrus clouds cover an estimated 16-20% of the globe and tend to consist of large, non-spherical ice particles (Liou 1986; Sassen et al. 2008). Figure 1.3 (Sassen et al., 2008) shows the global distribution of cirrus clouds in single- and multi-layer regimes; we can see that the highest frequency of high clouds occur in areas of deep convection, such as in the tropics near the intertropical convergence zone (ITCZ) and monsoonal regions, and in the mid-latitudes near mid-latitude storm tracks.

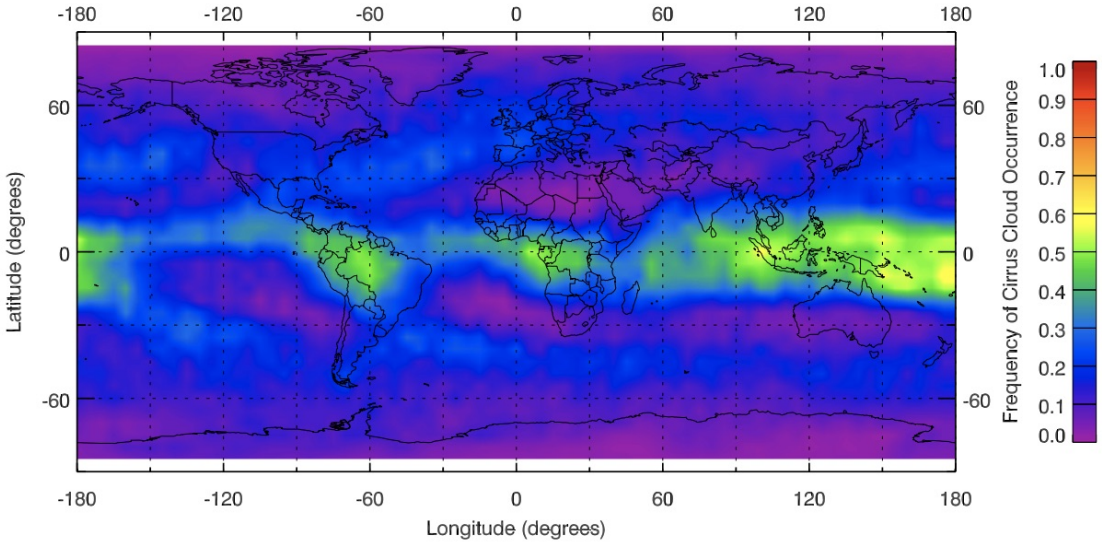

FIGURE 1.3: Global distribution of 1-year average frequency of occurrence of cirrus clouds identified by CloudSat/CALIPSO algorithm, with 5° latitude by 5° longitude grid boxes, daytime and nighttime measurements, and single and multiple cirrus layers (Sassen et al., 2008).

In order for these clouds to form, there needs to be available water vapor and cloud condensation nuclei (CCN) in the upper troposphere and some sort of mechanism

to initiate condensation and homogeneous nucleation. Some examples of cirrus and their formation mechanisms include synoptic cirrus, which form in association with jet streams and frontal low pressure systems; injection cirrus, which form from strong updrafts in deep convective clouds; mountain-wave cirrus, which form from orographically forced ascent; cold trap cirrus, which form in high altitudes in the tropics seemingly influenced by thunderstorm activity and other tropical wave disturbances; and contrail cirrus, which form from the rapid cooling of aircraft exhaust (Sassen et al., 2008). Due primarily to the relative scarcity of water vapor in the upper troposphere, these high cirrus clouds are generally rather transparent and optically thin, with optical depths usually below 3 and geometric thicknesses near 2 kilometers on average (Sassen et al., 2008). However, often cirrus clouds have much lower optical depths than this; for example, Sassen and Campbell (2001) found through a regional mid-latitude observational analysis that cirrus cloud optical depths did not exceed 0.3 for about half of the time for detected cirrus in their period of interest. The size of the ice crystals found in these high clouds can range between 10 and 1000 μm (Liou, 1986), although the typical effective diameter of ice crystals in cirrus clouds found in the mid-latitudes typically ranges between 10 and 100 μm (Ackerman and Stokes, 2003), and the ice water content of these types of clouds is typically on the order of 0.1 g m^{-3} (Liou, 1986). We will primarily be focusing on high level ice clouds in this analysis.

Low-level clouds are typically composed entirely of liquid droplets, whose base usually appears below 2 kilometers above the surface, or below 680 hPa, depending on your classification. Here, this classification includes stratus (St), stratocumulus (Sc), and

cumulus (Cu). These clouds are often shallow but can cover large horizontal extents (Wang, 2013). They also are often optically thick, due to the availability of water vapor near the surface for condensation, which increases their liquid water content; and due to the availability of cloud condensation nuclei near the surface, which increases the drop concentration and decreases the cloud effective radius. In the mid-latitudes, these clouds can be associated with light rain, drizzle, or snow. While the focus of this study will not be on low-level clouds, low-level clouds often provide the background for retrieving ice clouds in multi-layer cloud scenes. Thus, introducing these types of clouds is essential to gain a broader picture of the typical cloud patterns observed on a global scale and to better understand the make-up of typical multi-layer cloud scenes.

High and low clouds do not always occur separately; rather, multi-layer clouds are common, with high ice clouds above low liquid clouds. Figure 1.3 shows the general global distribution of single- and multi-layer cirrus clouds together. When we separate these high cirrus clouds into separate single- and multi-layer scenes, we see that most of the cirrus clouds observed are not isolated; rather, they occur in multi-layer cloud regimes. Figure 1.4 (L'Ecuyer et al., 2019) separates clouds observed globally into their different classifications, separating multi-layer cloud scenes from single-layer clouds scenes. Focusing on ice clouds, we see that single-layer cirrus clouds in this dataset have an annual mean cloud fraction of 7.9%, while multi-layer cloud regimes have an annual mean cloud fraction of 29.9%. While multi-layer clouds could involve a multitude of cloud combinations, when we partition those multi-layer cloud scenes into their high and low cloud components (Figure 1.5), we can see that cirrus clouds are the most common upper-level

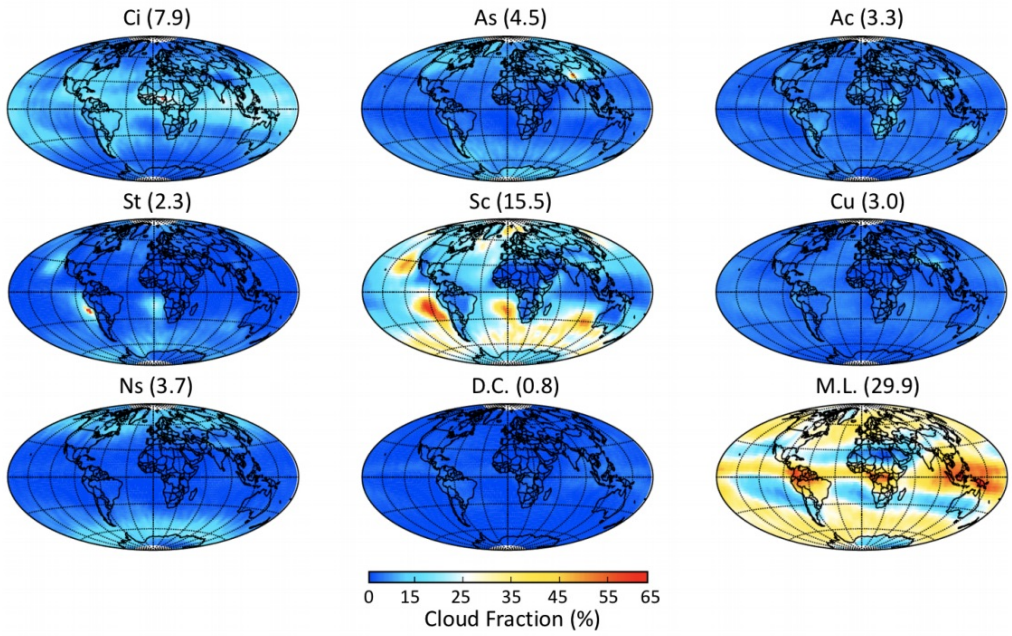

FIGURE 1.4: Breakdown of annual mean cloud fraction by cloud type determined based on CloudSat's 2BCLD classification, 2007-2010 (%). The area-weighted global average (in %) is shown in parentheses. Ci=cirrus, As=altostratus, Ac=altocumulus, St=stratus, Sc=stratocumulus, Cu=cumulus, Ns=nimbostratus, D.C.=deep convection and M.L.=multi-layered cloud system (L'Ecuyer et al., 2019)

cloud in multi-layer cloud environments in the mid-latitudes, while altocumulus or stratocumulus are the most common lower-level cloud in these environments (Hang et al., 2019). So, not only are high level cirrus clouds prevalent as single-layer clouds, but they are even more frequently seen in multi-layer clouds scenes above low-level liquid clouds.

A multitude of factors contribute to the formation and dissipation of clouds; however, two of the primary drivers of cloud formation are the large-scale general atmospheric circulation and localized dynamical processes, such as vertical air motions, deep convection, and mixing (Rogers and Yau, 1996) as seen in Figure 1.6 and Figure 1.7 (Boucher et al., 2013). The strong solar insolation at the equator initiates widespread convection

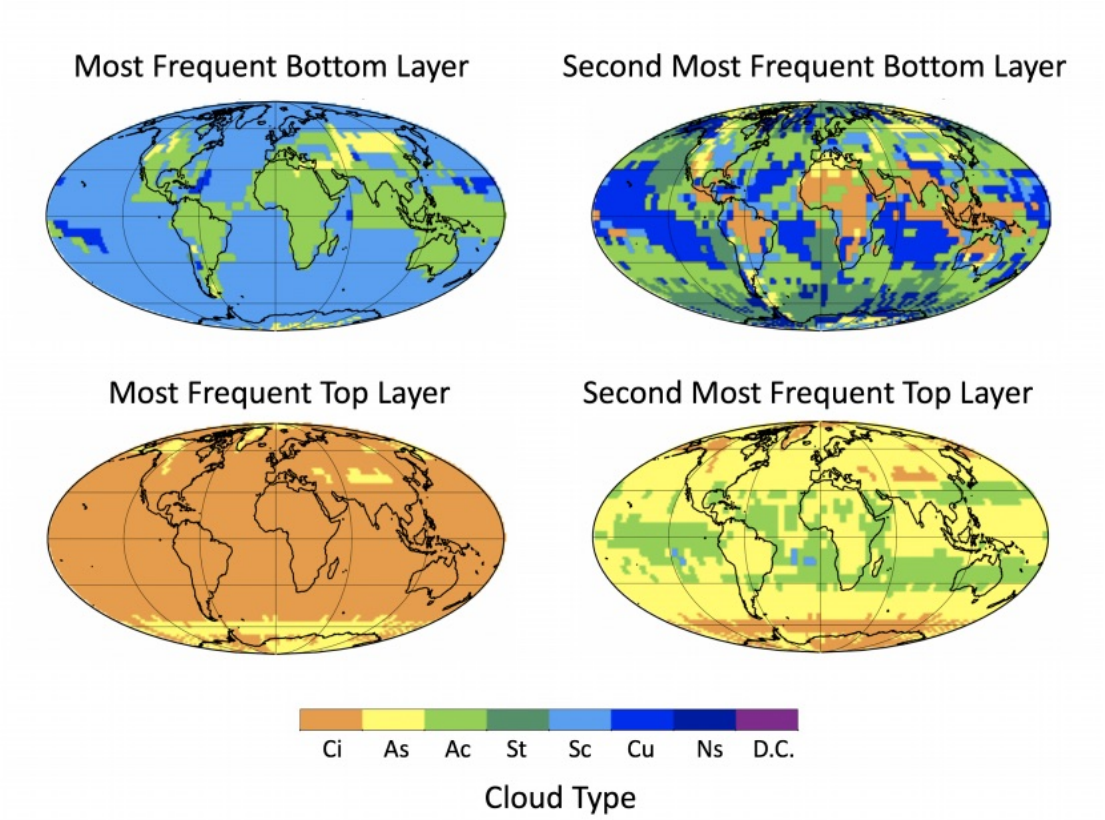

FIGURE 1.5: The most frequent and the second frequent cloud types identified as the bottom and top layers of multi-layered cloud systems (Hang et al., 2019).

and drives the tropical Hadley cell, which influences the cloud regimes seen in both the tropics and the subtropics (Figure 1.6c). On the ascending branch of the Hadley cell near the equator, we generally observe active areas of convection, which create a combination of shallow cumulus, deep convective clouds, and upper-level cirrus clouds that result from dissipating anvils and other large-scale weather disturbances (Sassen, 2002). On the descending branch of the Hadley cell in the subtropics, we typically observe low-level stratus, primarily in eastern ocean basins with a source of cool ocean water (Arakawa 1975; Klein and Hartmann 1993). The frequency of these tropical clouds can be seen in

Figure 1.7.

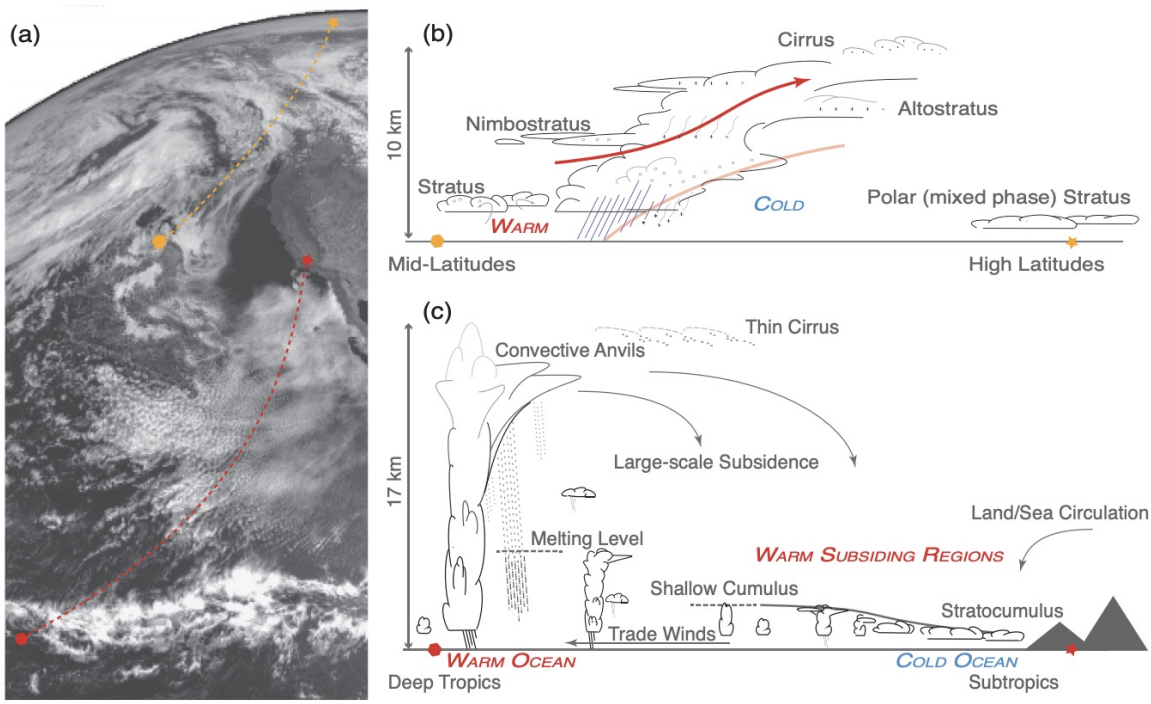

FIGURE 1.6: Cross sections of general circulation patterns and cloud regimes associated with them (Boucher et al., 2013).

In the mid-latitudes, baroclinic cyclones dominate the general circulation, and frontal ascent creates clouds spanning from shallow cumulus and stratocumulus to nimbostratus, cumulonimbus, and upper-level cirrus, most frequently along mid-latitude storm tracks (Figure 1.6b, Figure 1.7). In polar regions, the shallow polar cell primarily contributes to the development of low-level stratus clouds that vary seasonally with sea ice extent (Eastman and Warren, 2010). While other microscale and macroscale processes influence the condensation processes that create these clouds, atmospheric dynamics play a key role. However, in cases when the large-scale forcing is weak, such as with the formation of some cirrus clouds, localized dynamical processes remain important (Mace et al.,

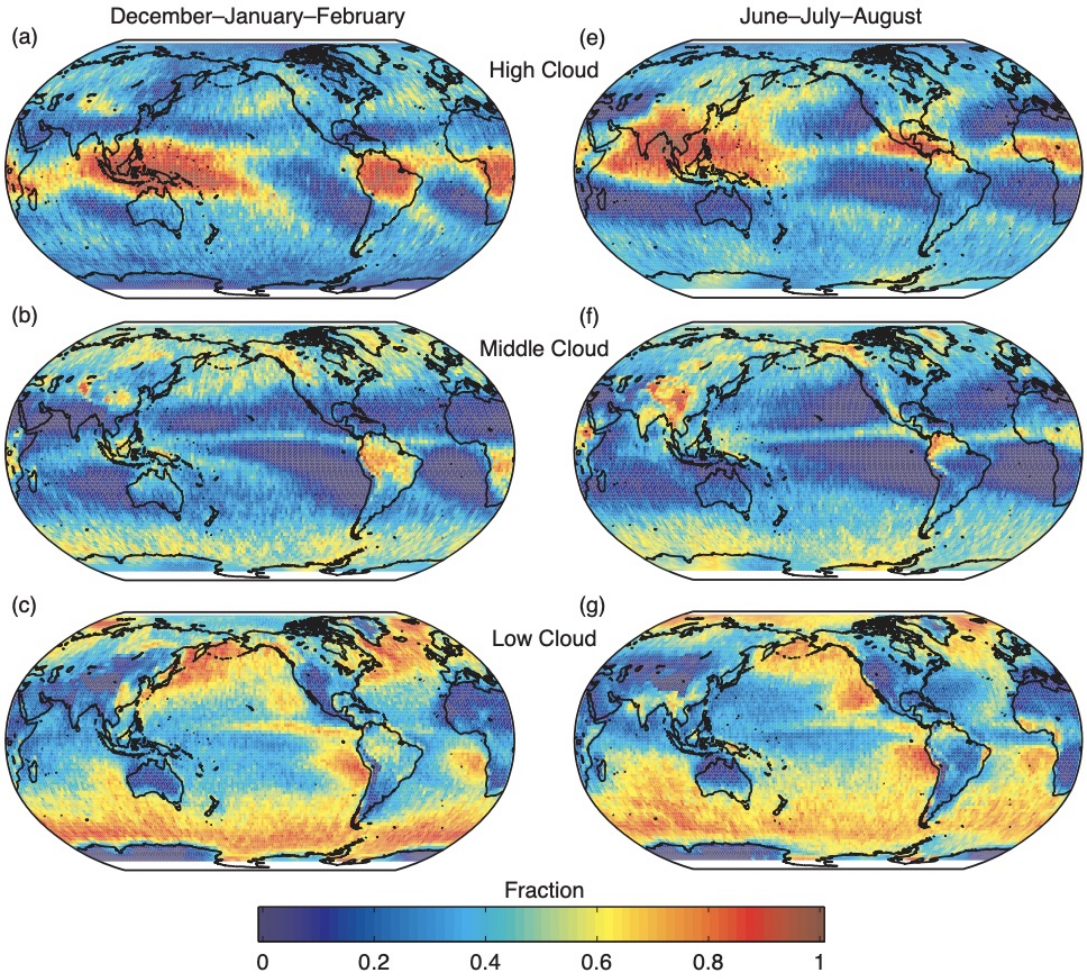

FIGURE 1.7: (a–c) December–January–February mean high, middle and low cloud cover from CloudSat/CALIPSO 2B-GEOPROF R04 and 2B-GEOPROF-LIDAR P1.R04 data sets for 2006–2011 (Mace et al., 2009); (e–g) same as (a–c), except for June–July–August (Boucher et al., 2013).

2001). Without localized processes such as turbulent mixing, condensation and freezing, and other microphysical processes, we would not be able to understand clouds as we do today.

However, clouds are not solely a product of atmospheric motions; rather, they in

turn work to influence the atmosphere around them through coupled dynamic, hydrological, and radiative processes such as the transport of atmospheric water vapor, redistribution of sensible and latent heat, and the modification of regional solar and infrared radiation balance (Arakawa 1975; Rogers and Yau 1996). Through this cycle, clouds act to influence the atmosphere and the global climate, which in turn adapts and responds by modifying the clouds present in the atmosphere. Understanding these cloud-climate interactions and feedbacks from various cloud types is essential to improving climate models and climate processes.

One of the primary influences that clouds have on the global climate is their ability to influence incoming and outgoing radiation beyond that of the clear atmosphere. The atmospheric absorption spectrum is displayed in Figure 1.8 (Marshall and Plumb, 2007). We see that the clear atmosphere absorbs a significant amount of outgoing longwave radiation, especially near the peak of infrared radiation emitted by the Earth. When looking specifically at the absorption by water vapor in the infrared spectrum, we see that water vapor is a near perfect absorber of infrared radiation, and must therefore be a near perfect emitter of infrared radiation as well, being in thermal equilibrium with its environment. When we incorporate clouds into our analysis, we see similar patterns. Figure 1.9 (Petty, 2006) shows an example of the scattering features of water and ice clouds. We see that in most of the shortwave spectrum, both liquid and ice clouds can rather effectively scatter shortwave radiation, while as we transition to the thermal infrared spectrum, clouds gradually become less effective at scattering and instead have higher absorption of infrared radiation (and higher thermal emissivity as a result).

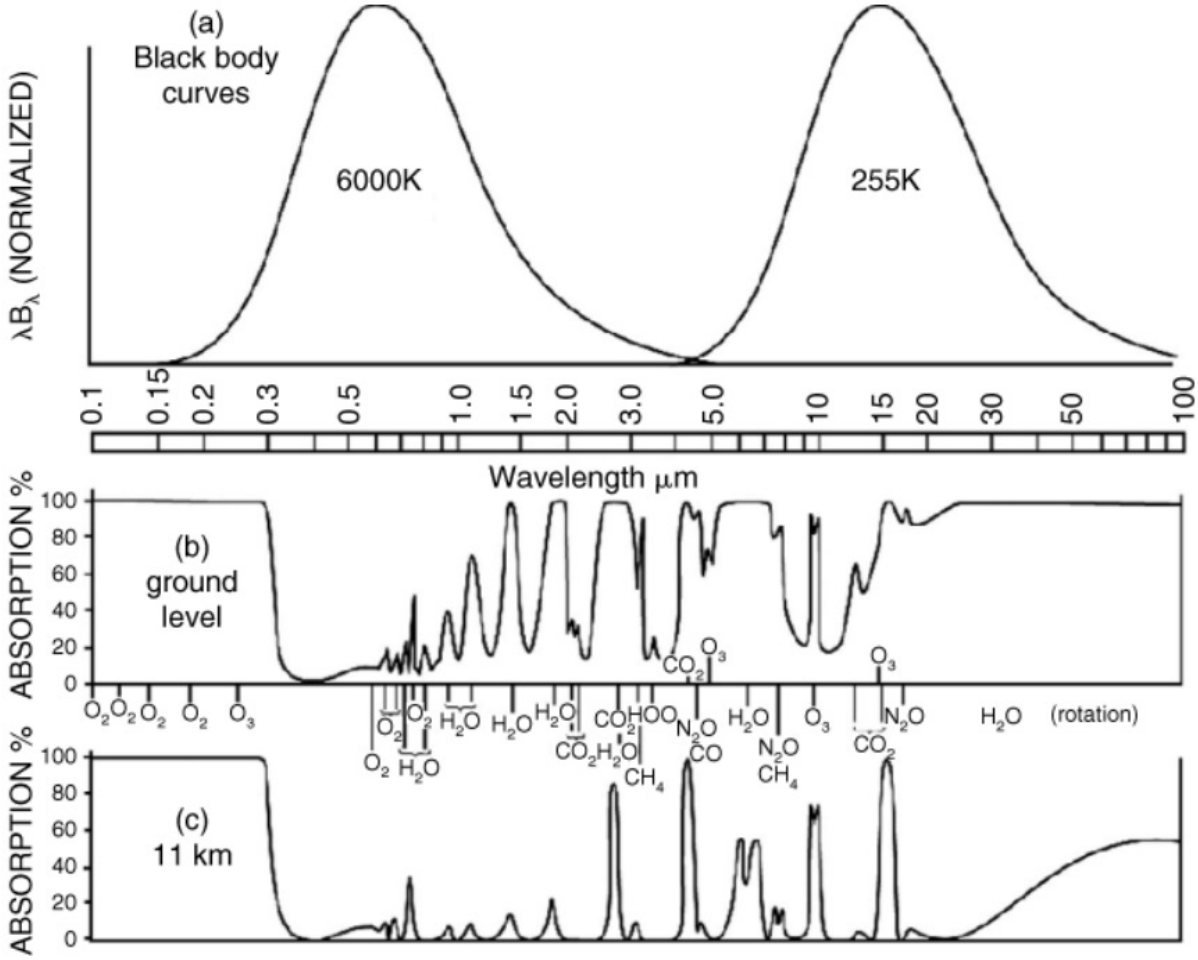

FIGURE 1.8: (a) The normalized blackbody emission spectra for the Sun (T = 6000K) and Earth (T = 255K) as a function of ln λ, where B_λ is the blackbody function and λ is wavelength. (b) The fraction of radiation absorbed while passing from the ground to the top of the atmosphere as a function of wavelength. (c) The fraction of radiation absorbed from the tropopause (typically at a height of 11 kilometers) to the top of the atmosphere as a function of wavelength (Marshall and Plumb, 2007).

The emissivity features of clouds can be confirmed and visualized with Figure 1.10 (Webster, 1994), which shows the relationship between cloud type and infrared emissivity. The broadband infrared emissivity of most cloud types is near unity, which indicates that most clouds behave like blackbodies in the infrared spectrum and are near perfect absorbers and emitters of infrared energy. The peak wavelength and the intensity of

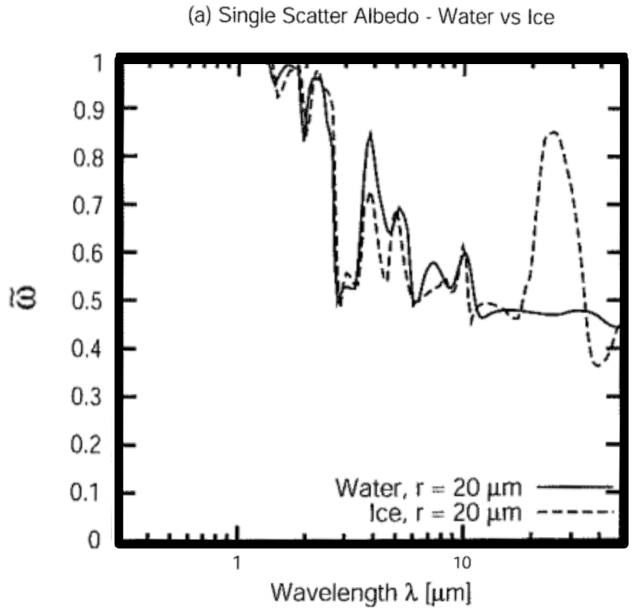

FIGURE 1.9: Single scatter albedo as a function of wavelength for water and ice spheres (Petty, 2006).

infrared emission by clouds are related to the temperature of the cloud, as evident by Wien's Displacement Law and Planck's Law, respectively, with cooler clouds emitting radiation that is both less intense and primarily at longer wavelengths than warmer clouds. This will become important when analyzing the differing radiative effects of clouds at different levels in the atmosphere. In summary, not only do clouds absorb a large portion of outgoing longwave radiation, they do so near perfectly, and thus can play a large role in the atmosphere's longwave radiative budget.

Looking again at Figure 1.9, we see that liquid and ice clouds scatter almost all and absorb little visible radiation, which is in the peak of emitted solar radiation. Since the absorption of visible radiation is near zero among both liquid and ice clouds, clouds will either reflect or transmit this type of shortwave radiation. The ability of clouds to

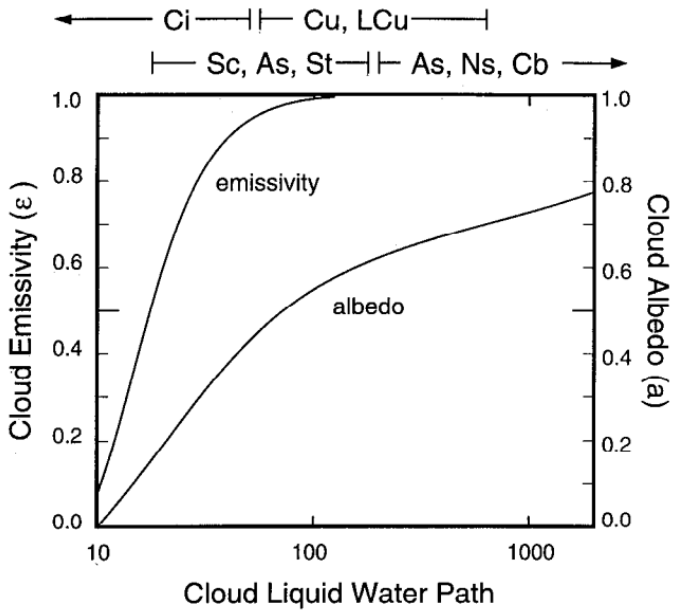

FIGURE 1.10: Relationship of the cloud albedo and emissivity as a function of the liquid water path of a cloud (Stephens, 1978). Cloud type with the values of liquid water path are shown on the upper abscissa. Whereas albedo increases relatively slowly with liquid water path, the emissivity increases rapidly. Thus, from the planetary surface, a cloud will appear to become optically black even for relatively thin clouds. The change in albedo grows at a slower rate with thickening clouds. (Webster, 1994)

reflect incoming solar radiation is modulated in part by a property known as cloud optical depth. Cloud optical depth is a non-dimensional parameter that describes a cloud's effect on the transmittance of light through the depth of a cloud. A cloud's optical depth is a function of its vertical extent, the concentration of liquid or ice within the cloud, and the size of the cloud particles, with the equation for optical depth below (Petty, 2006),

$$\tau \cong \frac{3LWP}{(2\rho r_e)} \tag{1.1}$$

where liquid water path (LWP) equals the liquid water content [LWC, (g m^{-3})] times the geometric thickness of the cloud (Δz). Its relationship to transmittance is also described

here,

$$t(z_1,\ z_2)\ =\ exp[\frac{-\tau(z_1,\ z_2)}{\mu}] \tag{1.2}$$

where $\mu = |cos(\theta)|$ and θ is the zenith angle. Here, we see that a cloud's optical depth is directly proportional to its liquid water path (or ice water path when the cloud is an ice cloud), and inversely proportional to the effective radius of the cloud. Furthermore, we see through eqn. 1.2 that as a cloud's optical depth increases, less radiation is transmitted through the cloud; it therefore must be either reflected or absorbed. Since clouds are generally poor absorbers of visible radiation (Figure 1.9), they have the tendency to reflect visible radiation, which is at the peak of incoming solar radiation. An exception to this is in the near infrared, for which absorption may be significant at some wavelengths. Furthermore, as a cloud's optical depth increases, it must reflect more incoming solar radiation, since the incident solar radiation is not being entirely absorbed or transmitted. This is shown in Figure 1.10, which shows that as a cloud increases in its liquid water path (or ice water path), its albedo increases, and it becomes more reflective of shortwave radiation.

Thus, we have learned that clouds are poor absorbers and good reflectors of visible radiation, and near perfect absorbers and emitters of thermal infrared radiation. These properties, however, depend on cloud type and optical depth. Generally, as evidence from Figure 1.10, clouds become more effective reflectors and absorbers, albeit at different rates, with increasing optical depth. The way that cloud radiative effects are quantified and the unique relationship between absorption and reflection for clouds at different heights in the atmosphere are described below. Here, we focus on clouds at lower levels

and clouds at upper levels, given that their opposing characteristics tend to also give them opposing radiative effects.

The manner in which different cloud types moderate the Earth's radiative balance can be quantified into a term called the cloud radiative effect (CRE), or cloud forcing. The cloud radiative effect (CRE) is defined below as the difference between the net clear sky flux and all sky flux (Hartmann et al. 1986; Ramanathan et al. 1989; Henderson et al. 2013):

$$CRE = (F_{upwelling} - F_{downwelling})_{clear} - (F_{upwelling} - F_{downwelling})_{all\ sky} \tag{1.3}$$

A positive net CRE at the top of the atmosphere indicates that clouds have a warming effect on the atmosphere, whereas a negative net CRE at the top of the atmosphere indicates that clouds have a cooling effect on the atmosphere. Based on various observational studies, the global and annual average net top of atmosphere (TOA) cloud radiative effect is near -20 W m^{-2} (Henderson et al. 2013; L'Ecuyer et al. 2019). However, as described above, regional cloud regimes contribute varying shortwave and longwave net CRE to the global average. Globally averaged, clouds tend to cool the climate system, despite regional variations in cloud type and height.

Knowing what we know about the impact of clouds on incoming solar and outgoing terrestrial radiation, as well as the general characteristics of clouds seen in the low and high levels, we can determine the effects that both high and low clouds have on the radiation balance. Single-layer low-level clouds tend to have a net cooling effect on the

atmosphere, with radiative effects ranging from -8.3 W m^{-2} to -1.3 W m^{-2} depending on the type of low-level cloud (L'Ecuyer et al., 2019). This occurs because being optically thick and bright, they have a tendency to reflect incoming shortwave radiation, as described above. In the thermal infrared spectrum, they absorb and emit almost all of the incident infrared radiation that they encounter. Since the cloud top temperature of low-level clouds is comparable to surface temperatures, these clouds emit comparable, albeit slightly less, upwelling thermal radiation than a scenario without the low-level cloud present. In other words, the emission temperature of low clouds is quite similar to that of the surface; thus, by Planck's Law, these clouds emit nearly equal amounts of longwave radiation as a clear-sky scenario. Compared to the cooling effect these clouds have from reflecting incoming solar radiation, their interference with net outgoing longwave radiation is small; thus, the dominant influence that low-level clouds have on the atmosphere is a cooling effect.

Single-layer cirrus clouds tend to have a net warming effect on the atmosphere of 2 W m^{-2} (L'Ecuyer et al., 2019). Due to their altitude and the relative scarcity of water and CCN available for ice particle growth, these high clouds tend to be optically thin, with lower concentrations of particles than low-level clouds. This leads to a lower albedo for these types of clouds, as shown in Figure 1.10. Furthermore, being higher in the atmosphere, the emission temperature of these clouds is much cooler than that of the surface. Thus, the radiation they emit is both at longer wavelengths and less intense than that from a clear-sky scenario. This means they have a much stronger greenhouse effect than lower level clouds, and thus the dominant influence that single-layer high level

clouds have on the atmosphere is a warming effect.

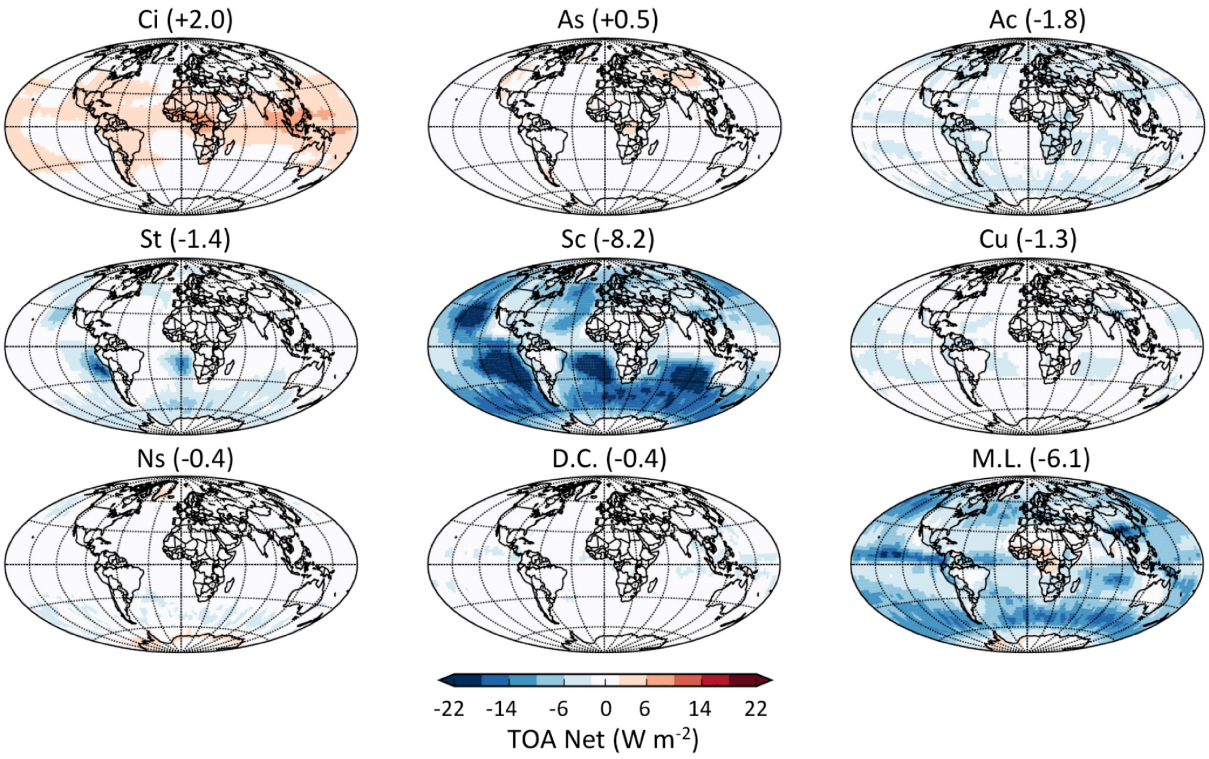

FIGURE 1.11: Annual mean net cloud radiative effects at the top-of-atmosphere (W m^{-2}). Radiative effects are separated by cloud type determined based on CloudSat's 2BCLD classification. All flux data presented are from CloudSat's 2BFLX algorithm, 2007-2010. The area-weighted global average (in W m^{-2}) is shown in parentheses. (L'Ecuyer et al., 2019)

However, in multi-layer scenes, the net radiative effect of the cloud column is negative, and these multi-layer environments tend to cool the planet by an average of -6.1 W m^{-2} (L'Ecuyer et al., 2019). This is due to the reflectivity of lower level clouds exceeding the greenhouse effect of the upper-level clouds, leading to an overall cooling effect of clouds in multi-layer scenes. Therefore, the radiative effect that upper-level ice clouds have on the atmosphere is cloud-scene dependent, and changes based on the number of cloud layers in the column. These radiative effects, based on cloud type, can be

seen in Figure 1.11 (L'Ecuyer et al., 2019).

While clouds on average work to cool the global climate system in the present, it is possible that clouds will have different net radiative effects in a warmer climate. When under the influence of a warming atmosphere, changes in cloud regimes have the potential to alter the Earth's radiative balance, influencing the net CRE on a global scale. The cyclical nature of these cloud-climate interactions can be depicted in Figure 1.12 (Schneider, 1972).

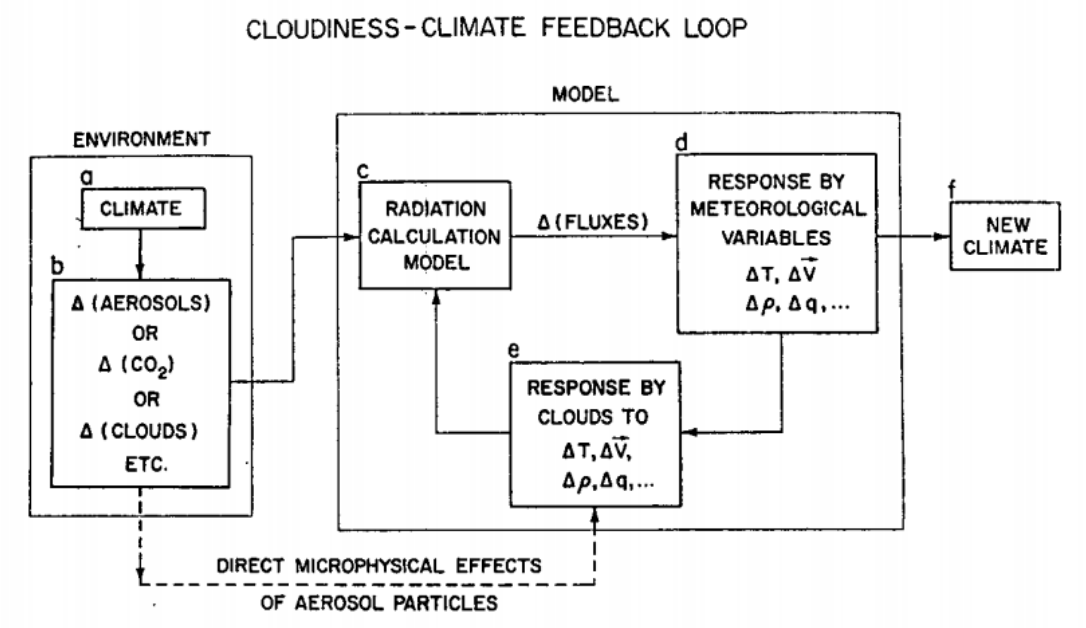

FIGURE 1.12: Flow chart illustrating the possible role of cloudiness as a climatic feedback mechanism. The arrows represent the order in which calculations would be made by a climate model attempting to predict the effect of changes in environment (e.g., ΔCO_2) on the climate (Schneider, 1972).

We see that a change in carbon dioxide, for example, (Figure 1.12b) creates a change in radiative fluxes and initiates a response by various meteorological variables, which in turn initiates a response by clouds and creates a feedback loop that continues

to change radiative fluxes and climate properties until an equilibrium is reached. The response by clouds to changes in atmospheric variables include geographic shifts to cloud regimes, vertical changes in cloud composition, and microphysical changes in response to changes in water vapor and aerosols. Here, we focus on the effects that a warmer climate has on the horizontal and vertical components of global cloud composition, as those are easier to analyze and model than changes in microphysical properties.

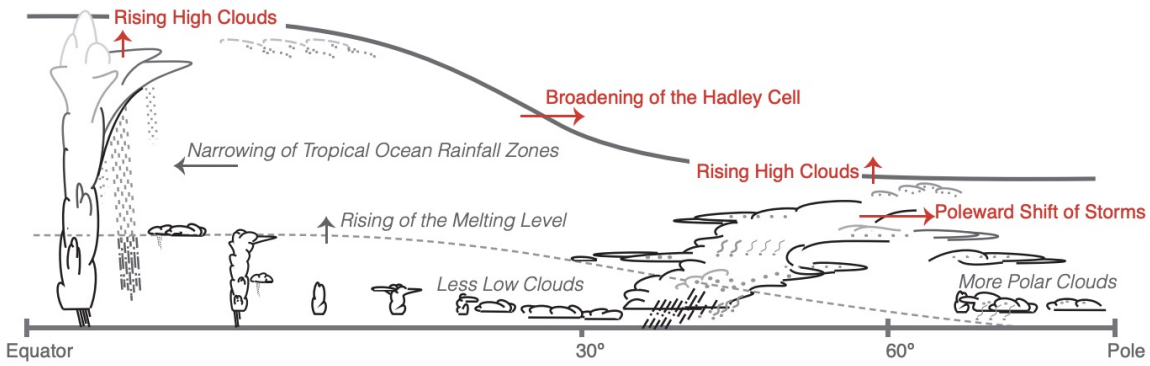

FIGURE 1.13: Robust cloud responses to greenhouse warming (those simulated by most models and possessing some kind of independent support or understanding). The tropopause and melting level are shown by the thick solid and thin grey dashed lines, respectively. Changes anticipated in a warmer climate are shown by arrows, with red color indicating those making a robust positive feedback contribution and grey indicating those where the feedback contribution is small and/or highly uncertain. No robust mechanisms contribute negative feedback. (Boucher et al., 2013)

Projected shifts in cloud regimes in a warmer atmosphere are depicted in Figure 1.13 (Boucher et al., 2013). A warmer climate has the potential to increase the height of high clouds in both the tropics and mid-latitudes, as the tropopause is projected to increase in height, which can allow clouds to form at higher altitudes (Santer et al., 2003). This can increase the greenhouse effect that high clouds impose on the atmosphere, since their emitting temperature becomes cooler (Schneider, 1972). Further projected cloud

changes include a broadening of the Hadley cell and poleward shift of the mid-latitude storm tracks. The broadening of the Hadley cell has the potential to influence the low-level stratus clouds observed over the subtropics, which are major contributors to the total negative CRE of single-layer low clouds and multi-layer clouds presently. The poleward shift of mid-latitude storm tracks has the potential to move clouds to areas with less sunlight, which will diminish their cooling albedo effect and limit their ability to reflect solar radiation in single-layer and multi-layer scenes. Furthermore, coupled with the expanding troposphere and the increasing height of mid-latitude clouds, the CRE of mid-latitude clouds could become more positive. Changes in cloud amount do not necessarily always imply changes in the Earth's radiative balance, since changes in high and low cloud amounts and locations can have opposing radiative effects and other cloud-climate feedbacks may be at play besides those mentioned here, such as interactions with aerosols (Schneider, 1972). However, some of these projected changes in cloud amount, specifically related to single-layer high clouds, could have a positive radiative effect and amplify atmospheric warming; thus, those feedbacks are essential to analyze for improving climate projections.

In order to quantify the effects of changing cloud regimes in a warmer climate, we need accurate measurements of clouds in the present, specifically of upper-level ice clouds in single- and multi-layer environments. Specifically, focusing on multi-layer cloud retrievals is essential to reducing uncertainty with climate projections, as these multi-layer clouds tend to occur more frequently than single-layer cases. Furthermore, these multi-layer clouds tend to be poorly resolved in climate models and joint observational

datasets, due to inherent incompatibility with single-layer cloud retrieval algorithms and various other multi-layer issues, such as problems with distinguishing between distinct upper and lower cloud layers and single-layer mid-level clouds (Zhang et al. 2005; Bodas-Salcedo et al. 2014). While a variety of ground-based stations are available worldwide with cloud-measuring instruments, these stations are not ideal for compiling a global distribution of clouds and are instead more useful for regional analyses. Rather, satellite retrievals would be better suited for this task; their global extent and their ability to measure multiple radiative and microphysical properties of clouds make them ideal for retrieving global cloud properties. The inherent problem of using conventional remote sensing techniques for the retrieval of multi-layer clouds is two-fold. First, passive instruments tend to lack the ability to measure the vertical structure of clouds at high resolutions or delineate various cloud boundaries in a multi-layer cloud scene (Mace et al. 2009; Mace and Wrenn 2013). Second, active instruments, while having better vertical resolution, lack the horizontal coverage that passive sensors have and can have issues with detecting low-level clouds due to attenuation near the surface. Despite these issues, working through these observational difficulties and attempting to improve the detection of these single- and multi-layered ice clouds is necessary to improve climate models and decrease the uncertainty associated with climate change projections.

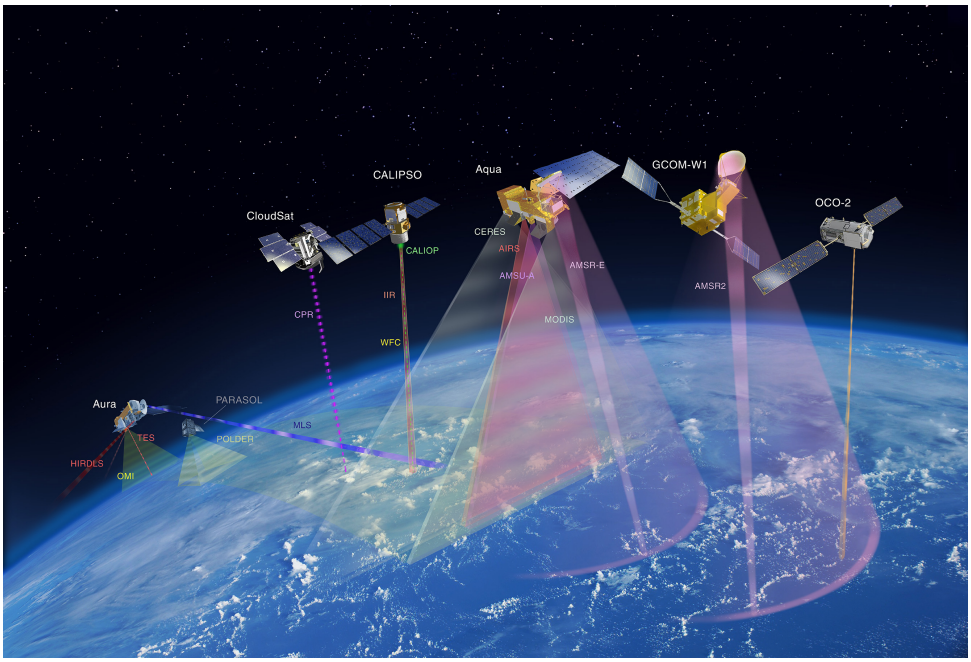

FIGURE 1.14: An illustration of NASA's Afternoon Constellation (A-Train) satellite mission with the satellites' respective instruments. Illustration courtesy of NASA.

1.2 A-Train Constellation and AIRS

The Afternoon Satellite Constellation (also known as the A-Train) contains a convoy of satellites with a multitude of active and passive sensors that measure key components of the atmosphere and improve our understanding of the processes that affect climate (NASA 2003; L'Ecuyer and Jiang 2010). The formation of these satellites allows for various collocated and synergistic measurements, meaning that more information about the condition of the Earth is obtained from the combined observations than would be possible from the sum of the observations taken independently (NASA, 2003). The tools on these satellites help evaluate the accuracy of climate models and how well they represent present-day atmospheric processes, such as the water cycle, surface-atmosphere

exchange, energy balance, and the composition of the atmosphere, specifically related to greenhouse gases, aerosols, and clouds. Without accurate representation of present-day atmospheric processes, climate model projections remain uncertain; thus, confirming their accuracy with observations is essential. Beyond climate model validation, this constellation of satellites can also provide data for present-day research, weather forecasting, and policy making, and thus is an essential source of data for environmental monitoring and policy.

NASA describes the A-Train constellation as follows:

> NASA and its international partners operate several Earth-observing satellites that closely follow one another along the same (or very similar) orbital "track." A particular example of a coordinated group of satellites are in a sun-synchronous polar orbit, crossing the equator in an ascending (northbound) direction at about 1:30 PM local solar time, within seconds to minutes of each other—hence the name Afternoon Constellation. This allows near-simultaneous observations from a wide variety of instruments that are synergistically used to aid the scientific community in advancing our knowledge of Earth-system science and applying this knowledge for the benefit of society. (https://atrain.nasa.gov)

The original A-Train satellites included Aqua (launched in 2002), Aura and PARASOL (launched in 2004), CloudSat and CALIPSO (Cloud-Aerosol Lidar and Infrared Pathfinder Satellite Observation, launched in 2006), and later included GCOM-W1 (2012) and OCO-2 (2014). The PARASOL satellite eventually dropped out of the A-Train orbit and ceased operations in 2013, and CloudSat and CALIPSO lowered orbits and exited the A-Train constellation in 2018, now forming their own C-Train constellation at a lower altitude. These satellites each are suited with a variety of instruments aimed at measuring specific properties of the atmosphere that when analyzed together, can paint a more

accurate and complete picture of the Earth's atmospheric processes.

The Aqua satellite, aptly named, focuses on the study of water in the earth system; it carries six instruments that retrieve properties about water in the atmosphere, temperature profiles, aerosols, land surface properties, radiative fluxes, and many other aspects of the global climate system (Parkinson et al., 2006). With a period of 98.8 minutes and a repeat cycle every 16 days, this satellite brings in nearly 90 gigabytes of earth system data per day. While it carries a variety of instruments, such as microwave sounders and radiometers, one that has been used frequently for the study of cloud properties is the Atmospheric Infrared Sounder (AIRS). The AIRS instrument is a high-spectral-resolution grating spectrometer that contains 2378 channels that measure infrared radiation at wavelengths from 3.74–15.4 μm (Parkinson et al., 2006). This instrument has a spectral resolution of $\lambda/\Delta\lambda \approx 1200$ nominal, and an NEdT at 250 K of 0.07–0.40 K from 3.75–11 μm and 0.27–0.68 K from 11.75–15.4 μm (https://airs.jpl.nasa.gov/mission_and_instrument/instrument/specs). Combined with a 13.5 kilometer resolution at nadir and a swath width of about 800 kilometer on each side of the ground track, the AIRS instrument is able to collect very high-resolution infrared radiance data over a large section of the Earth at once. This radiance data can be used to detect clouds in the atmosphere, due to the manner in which they influence the outgoing radiation, and the high-spectral-resolution of this instrument can be utilized near atmospheric absorption bands to derive vertical profiles of atmospheric variables, despite being a passive and non-probing instrument.

Other essential A-Train satellites that have been used for the retrieval of cloud

properties are the CloudSat and CALIPSO satellites. Now located in the C-Train constellation, these two satellites contain active instruments essential for the retrieval of the vertical structure of clouds. The CloudSat satellite contains onboard a 94-GHz cloud profiling radar (CPR) with 500-meter vertical resolution from 0-25 kilometers above the surface, which can detect over 80% of liquid water clouds and over 90% of ice clouds (NASA, 2003). The CALIPSO satellite contains onboard a lidar instrument called CALIOP (Cloud-Aerosol Lidar with Orthogonal Polarization), a nadir pointing dual-wavelength polarization lidar at 532 nanometers and 1064 nanometers, with a horizontal resolution of 30 meters from 0-40 kilometers above the surface and a footprint spacing of 333 meters along track (NASA, 2003). The CALIOP instrument is able to provide more information about the phase of the water present in the cloud, the boundaries of cloud layers in the atmosphere, and the particle size of cloud droplets, providing complementary information to CloudSat and other A-Train satellites. Together, these satellites are able to measure the properties of a variety of clouds observed worldwide in the atmosphere. However, their high vertical resolution comes at a cost of horizontal coverage, and their horizontal swath is nothing compared to that of infrared sensors in the A-Train constellation, which is why we are focusing on the AIRS instrument in this analysis.

We chose to focus on the AIRS instrument in this analysis rather than other infrared sounders (namely IASI and CrIS) because of the nature of the A-Train instruments and the opportunities for joint retrievals among the A-Train instruments. Joint retrievals among the AIRS instrument and other active and passive co-located A-Train instruments can increase the confidence in the types of observed global cloud scenes. While we do

not attempt to combine measurements from other A-Train instruments here, we believe that analyzing the way we use the AIRS instrument can improve joint retrievals with other A-Train sensors in the future. However, repeating this analysis for other infrared sounders, such as IASI and CrIS, could lead to some interesting insights due to differences in the way these sensors make atmospheric measurements (Smith et al., 2015). Namely, these instruments are not grating spectrometers like AIRS; rather, both IASI and CrIS are Fourier transform spectrometers, which do not have issues with bad channels like the AIRS instrument, an issue we will discuss later in this analysis.

1.3 Current Research on Satellite Retrievals of Cloud Properties

Retrieving properties of clouds from satellites is no easy task and depends on the surface type over which the clouds reside, the number of cloud layers, the time of day, and the various properties of the clouds, including their thickness, altitude, particle size, and ice or liquid water content. Generally, the process of cloud retrieval involves identification of the cloud and retrieval of its properties. The first process of identifying a cloud can involve comparing observed TOA radiances from passive satellite instruments to those expected in a cloud-free atmosphere to see if clouds are present and their large-scale structure (Minnis, 2002). From there, the measured signal needs to be processed to determine what cloud properties could create the radiances observed across wavelengths. Often, radiative properties of water, such as emissivity and reflection; absorption features

of atmospheric constituents, such as carbon dioxide; and differences in radiances in infrared window channels are exploited to infer the properties of clouds in a column from passive instruments (Stephens and Kummerow, 2007). For example, known differences in scattering features across the infrared spectrum among liquid and ice clouds can be exploited to infer the phase of observed clouds (Figure 1.9). Retrieving cloud properties can also be done with active instruments, such as cloud radar or lidar, to measure the internal structure of clouds. From active instruments, such as the 94 GHz cloud radar on CloudSat and the CALIOP lidar instrument on CALIPSO, more direct measurements of cloud properties are possible. The 94 GHz cloud radar, like that on board CloudSat, is at a frequency that has a local minimum in absorption by atmospheric constituents across varying humidities (Lhermitte, 1988). Its beam is also able to extend deep into the atmosphere to measure the properties of near-surface layer clouds (Lhermitte, 1988), which gives a more complete picture of all of the clouds present in the atmosphere. The time and direction of the backscattered radar echo can yield insight into the location of cloud droplets in the column, whereas the strength of the signal can yield insight into the size and kind of cloud particles present (Wang, 2013). Lidar is able to complement radar measurements by utilizing visible light instead of microwave. Since visible light cannot penetrate through thick clouds, lidar is often used for the detection of cirrus clouds (Wang, 2013). Dual-polarization, such as that found on CALIOP, can provide insight into the shape of the cloud particles, which can be useful when the phase or type of cloud droplet is ambiguous. Comparing cloud retrievals of active and passive sensors,

specifically retrievals of cloud top height, shows broad agreement among these various active and passive instruments, although inconsistencies can arise from retrieval algorithm differences and instrumentation differences (Weisz et al., 2007).

Once we identify spectral regions that contain information about the cloud properties of interest, the measurements from these channels need to be processed. This can occur through retrieval algorithms based on theory or empirical data analysis, inverse methods such as optimal estimation, or others types of algorithms, such as the operational AIRS retrieval method (e.g. Kahn et al., 2014) or the dual regression algorithm, (Weisz et al. 2011; Smith et al. Smith et al.) which can retrieve vertical cloud and thermodynamic profiles under all sky conditions in near-real-time. Some of these methods involve using a cloud-clearing retrieval, which derives non-cloud-related atmospheric parameters from "clear sky" radiances that are estimated from various linear combinations of channels sensitive to clear-sky properties, as well as optimal estimation, which is used to retrieve cloud optical depth, particle size, and cloud temperature.

1.4 Shortcomings

Ice clouds, in single-layer and multi-layer regimes, can be difficult to observe; the thermal contrast between clouds and their surroundings is very low, which makes ice cloud retrievals challenging, especially with infrared instruments alone. Furthermore, their subgrid-scale nature does not help the retrieval process. As a result, large discrepancies exist in global datasets and climate models related to their properties (Eliasson et al., 2011). Observations of these upper-level ice clouds can be impacted by the spectral domain of

the instrument measuring them (Stubenrauch et al., 2013), which can be sensitive to clouds in various atmospheric layers and can make retrieving and distinguishing clouds in multi-layer environments challenging. Furthermore, conventional observation systems have their limitations; while active sensors, specifically those found in the A-Train constellation, are often able to retrieve high-resolution information about upper-level ice clouds in single- and multi-layer environments, they lack the same areal coverage as passive sensors, whose swath width is on the order of hundreds of kilometers, and can have issues with attenuation, which can be a problem for measuring multi-layer clouds. And while passive sensors cover larger swaths of the Earth than active sensors, their resolution and inability to directly probe the atmosphere in the same way as active sensors can pose problems for cloud retrievals. There is room for growth in retrievals using both active and passive instruments, and optimizing the measurements we attain from these instruments will improve our understanding of global ice clouds and their radiative effects in single- and multi-layer environments.

1.5 Research Questions

Through this study, we are looking to supplement satellite retrievals of mid-latitude ice clouds by focusing on which AIRS channels are often most sensitive to the properties of thin, upper-level ice clouds, particularly to their cloud top temperature, optical depth, and particle size. We are interested in learning what combinations of AIRS channels yield the most information about high-altitude ice cloud properties in the mid-latitudes; furthermore, we are looking to see how channels with the most information change in

multi-layer cloud environments, where lower, liquid clouds are present. We find that there are some similarities and differences between the AIRS channels that contain the most information about ice clouds in single-layer and multi-layer cloud scenes; those details will be explored in this analysis.

Chapter 2

Methodology

A summary of the methodology used in this study is as follows. We employed a radiative transfer model (RTM) to simulate the top-of-atmosphere infrared radiances that would be observed if a variety of ice clouds were in a general mid-latitude atmosphere. The ice clouds we analyzed were derived from a 6-year database of ice clouds observed over the Atmospheric Radiation Measurement program's Southern Great Plains (ARM SGP) site. We took this extensive ice cloud database and used a clustering algorithm to cluster together clouds with similar properties to narrow down that database, with each derived cluster being representative of a larger group of observed ice clouds. To address the question of how low clouds influence ice cloud retrievals, we added in low-level liquid clouds of varying optical depths beneath each ice-cloud cluster to simulate multi-layer cloud environments and see how these low-level liquid clouds influence the top-of-atmosphere radiative budget and optimal channel selection for ice-cloud retrievals. From here, we

used the AIRS spectral response function to convert the simulated radiances from the radiative transfer model into simulated measurements from the 2378 channels on the AIRS sensor. Finally, we calculated the information content of each of the simulated channel measurements to see which AIRS channels were generally most sensitive to the properties of the ice-cloud clusters that we simulated in the RTM from both single- and multi-layer cases. The specifics of each of these steps are described below.

2.1 Radiative Transfer Model

The radiative transfer model used in this analysis is based on the Vector Linearized Discrete Ordinate Radiative Transfer (VLIDORT) model (Spurr, 2006) to simulate radiances and Jacobians from the cloudy scenes that we prescribe it. The High-Resolution Transmission Molecular Absorption (HITRAN) database (Rothman et al., 2009) was used for gas attenuation, and the methodology of Bodhaine et al. (1999) is used for the treatment of Rayleigh scattering. This model simulates line-by-line radiances and Jacobians, which were processed with the AIRS spectral response function to simulate the radiances observed by the AIRS instrument. Here, we assume that all of the cloudy scenes are overcast (100%), and we assume daytime conditions. Our simulations were carried out with a grass surface, with a spectral emissivity derived from the Advanced Spaceborne Thermal Emission Reflection Radiometer spectral library (Baldridge et al., 2009) and an ocean surface, with a spectral emissivity derived from Hale and Querry (1973) and Sidran (1981). We used a constant solar zenith angle of 10 degrees and a viewing angle of 30 degrees. In our analysis, surface type had negligible influence on the channels selected as

containing the most information about the single-layer and multi-layer cloud properties; this result is consistent with other information content analyses of the AIRS instrument (Chang et al., 2017). Furthermore, Chang et al. (2017) found that differences between viewing angles had negligible effects on AIRS channel selections; thus, we only considered one viewing angle in our analysis.

We used one standard background atmospheric profile in our analysis and integrated the clouds we wished to observe into this profile. The atmospheric thermodynamic and aerosol profile was compiled using a combination of a modeled atmospheric profile and reanalysis data. The vertical resolution of the atmospheric profile was 500 meters from the surface up to 20 kilometers; from here, the profile extended in layers up to 10 hPa. The profile of temperature, pressure, and atmospheric gases was compiled using the US Standard Atmosphere (Anderson et al., 1986) and MACC reanalysis data (Inness et al., 2013), taken over the SGP site. The MACC reanalysis dataset is from 2003–2010 and contains reanalysis data of atmospheric constituents compiled from a variety of global observational datasets. Here, we took the mean of the reanalysis data over the SGP grid box, coupled it with the US standard atmosphere temperature and pressure levels, and interpolated it to a grid with 500-meter vertical resolution from the surface up to 20 kilometers, with additional levels up to 10 hPa. We then were able to take each of the ice cloud clusters and integrate them into the atmospheric profile based on their cloud top pressure and thickness of the cloud.

With our radiative transfer calculations, we assumed various sources of error related to the AIRS instrument, assumed temperature and water vapor profile, ice crystal

habit, and aerosols, which we derived from Chang et al. (2017) and will describe more extensively when we describe how we calculate information content.

2.2 Cloud Database

The Atmospheric Radiation Measurement (ARM) program hosts a variety of active and passive ground-based instruments that monitor atmospheric variables that influence the Earth's radiative fluxes, with a specific goal of increasing our understanding of the interaction between clouds and atmospheric radiative fluxes and improving the representation of clouds in global circulation models (Ackerman and Stokes, 2003). This program has compiled years of data at various tropical, mid-latitude, and polar sites worldwide. Here, we used observational data measured from the Southern Great Plains (SGP) site, with a suite of instruments centered in Lamont, OK that measured atmospheric properties. For this study, we consider the ice clouds observed here to be representative of the ice clouds observed in the mid-latitudes; however, this analysis could be repeated using ice clouds over ocean to create a more robust mid-latitude ice cloud dataset. The data used in this study was collected from the SGP site from 2003–2009, with a 5-minute temporal scale and 90-meter vertical resolution.

The occurrence, vertical structure, and microphysical properties of clouds at this site are recorded by vertically pointing active ground-based sensors at the SGP central site (Mace et al., 2006). This includes laser ceilometers, a micro-pulse and Raman lidar, and a millimeter radar (MMCR). The laser ceilometer is used to denote cloud base in the middle and lower troposphere; these observations are combined with observations from

the MMCR to characterize the vertical profile of cloud properties. The MMCR is able to record the radar reflectivity factor, the Doppler velocity, and the Doppler spectrum width. These measurements are then plugged in to a hierarchy of algorithms to create profiles every 36 seconds, which then are averaged into the 5-minute temporal resolution that exists in the dataset, as described in Mace et al. (2006). Specifically, the cloud properties we focused on here for the upper-level cirrus clouds were the effective radius, ice water content, cloud top temperature, cloud top pressure, and geometric thickness. To derive ice water content, while a hierarchy of algorithms and parameterizations are used at this site, we used the Liu and Illingworth (2000) algorithm for this quantity, as this was the most reliable after data processing and quality control. This retrieval scheme relates radar reflectivity to ice water content, and was the first in the hierarchy of algorithms that produced all realistic values for both ice water content and effective radius. The atmospheric thermodynamic profiles were derived from the radiosonde record from the SGP central site, and merged with nearby radiosondes and model data when needed. With these ground-based sensors, we are able to create a continuous dataset from 2003–2009 of the ice clouds observed at this site, with detailed information about their microphysical and thermodynamic properties. From here, we were able to narrow down the clouds seen by only choosing top-layer ice clouds, whose cloud top temperature was below -20°C to get our dataset of upper-level ice clouds used in this study. In this period, we were able to extract $1.4 \cdot 10^5$ cloud profiles of ice phase below -20°C, with properties visualized in Figure 2.1. We consider these clouds to be representative of general mid-latitude ice clouds.

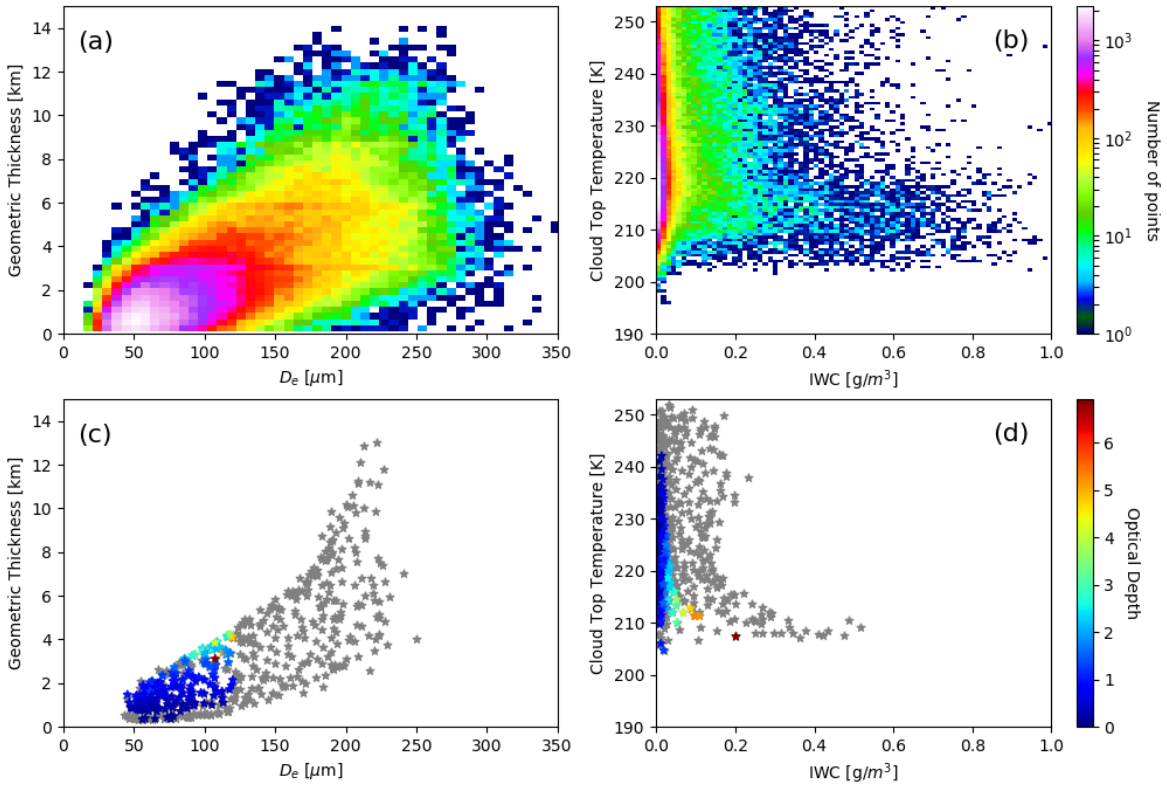

FIGURE 2.1: (a) Density plot showing the geometric thickness and effective diameter (D_e) of the ice cloud profiles derived from the ARM SGP site from 2003–2009. (b) Density plot showing the cloud top temperature and ice water content (IWC) of the ice cloud profiles derived from the ARM SGP site from 2003–2009. (c) The geometric thickness and effective diameter (D_e) of the ice cloud profiles from the ARM SGP site after clustering. Each point represents one of the 500 cloud clusters; the grey points were cloud clusters that were not analyzed, while the shaded clusters represent the 156 cloud clusters that were analyzed, shaded by the optical depth of the cluster. (d) Same as (c), but showing the cloud top temperature and ice water content (IWC) of the ice cloud profiles from the ARM SGP site after clustering.

2.3 Clustering Algorithm

Simulating the radiances of all of the single-layer clouds retrieved from the ARM SGP site would be computationally intensive. Furthermore, with the aim of this study to improve retrievals of ice cloud properties in the mid-latitudes as a whole, modeling the specific TOA radiances with each individual ice cloud observed at this site would not be

useful, as the likelihood of those specific clouds with their specific thermodynamic and microphysical properties to reoccur in the future is extremely low. For these reasons, the extracted cloud layers from this site were clustered using the non-hierarchical k-means clustering algorithm (Wilks, 2011). The input into this algorithm is the cloud dataset from the ARM SGP site, with values of cloud top temperature, effective particle size, geometric thickness, cloud top pressure, and ice water content for each cloud, and a predetermined number of centroids, with random values of these cloud variables assigned to them. The Euclidean distance between each of the initialized centroids and each cloud point in the dataset is calculated, and the cloud point is then assigned to the closest centroid, that therefore has more similar cloud properties to the observed cloud point than the other centroids. Once each point is assigned to a centroid, the centroid's position (and cloud variables) are then updated to the mean of the points that are assigned to it. The process repeats until each point, which represents an observed cloud measurement, is closest to its cluster mean and a full cycle reiteration produces no reassignments.

Here, the number of centroids chosen was subjective; the goal was to find the number of clusters that seems to capture a majority of the range of characteristics included in the observed SGP cloud dataset; for this study, the $1.4 \cdot 10^5$ single-layer ice cloud profiles were reduced to 500 centroids. Once these centroids were determined, we calculated the central optical depth of each centroid and compared it to the optical depths of the observed cloud points assigned to each centroid. If the centroid's central optical depth was less than the standard deviation of optical depths assigned to that cluster center, we filtered that cluster center out. Furthermore, centroids were filtered based on their effective

diameter; only centroids with diameters between 10 and 120 microns were considered, due to the limitations of the ice crystal scattering property dataset (Baum et al., 2014). This left us with 138 initial ice cloud cluster centers to analyze and simulate, with a range of properties shown in Figure 2.1 and Figure 2.2. Because this filtering technique left us with very thin clouds with optical depths below 2.5, we ended up loosening our restrictions to analyze clouds with larger optical depths. We analyzed 18 extra clusters with optical depths above 2.5 by loosening the restriction so that the cluster's central optical depth be greater than 1.5 times the standard deviation of the optical depths of the cluster points assigned to it. While this indicates that the clouds represented by these clusters have a larger spread, we believe that analyzing these additional clusters will expand the range of applicability of the results to more completely cover the spectrum of cirrus cloud regimes observed in the mid-latitudes. This left us with a total of 156 ice clusters that we analyzed.

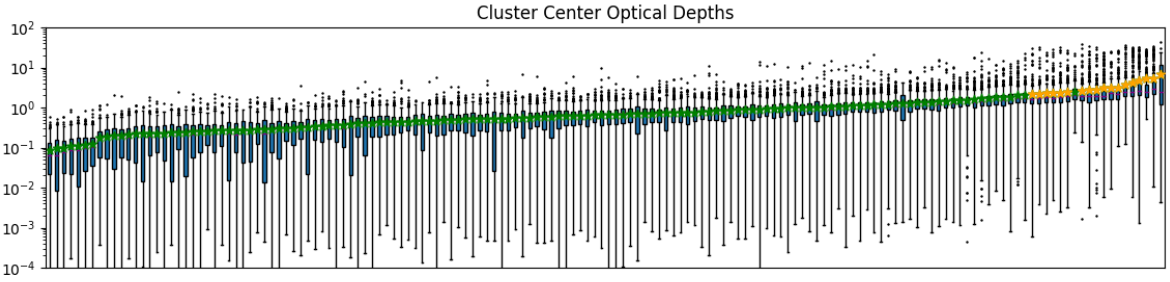

FIGURE 2.2: Box-plots for each of the 156 cloud clusters analyzed in this study, mapping the optical depths of all of the points associated with each cluster center. The central optical depth of each ice cloud cluster is plotted on top of the box-plots. The green stars indicate that the standard deviation of optical depths among the points associated with each cluster was less than the central optical depth, while the yellow stars indicate that the standard deviation was larger than the central optical depth.

Figure 2.1 compares the characteristics of the observed cloud profiles from the SGP site to the characteristics of the cloud clusters we analyzed in this study. We can see that the cluster centers we chose to analyze are representative of the cloud properties most frequently observed at the SGP site. Generally, we can see that the majority of the ice clouds have a geometric thickness less than 3 kilometers, effective diameters less than 100 microns, and ice water contents less than 0.1 g m^{-3}; these characteristics are echoed in the 156 cloud clusters that we derived and analyzed. Figure 2.2 plots out the optical depths of the clusters we chose to analyze. A majority of the clusters we chose to analyze have optical depths below 1, with all optical depths falling below about 7. This indicates that most of our clouds are optically thin, and their other properties fall in line with other general observations of cirrus clouds (Sassen and Campbell 2001; Sassen et al. 2008). In Figure 2.2, the clusters that we loosened our optical depth restrictions for are highlighted; we can see that the spread of cloud optical depths associated with each of these 18 clusters is large, and the central optical depth is therefore not necessarily the best representation of the clouds associated with it. However, we believe that for now, these clouds should still be analyzed until a more robust method to study optically thick ice clouds is determined.

2.4 Liquid Cloud Database

While the purpose of this study is to improve retrievals of upper-level ice clouds in the mid-latitudes, we know that these types of clouds are not always isolated. Rather, multi-layer clouds, with cirrus layers in the upper levels and liquid cloud layers at lower levels

are rather frequent (L'Ecuyer et al., 2019). Thus, liquid clouds were introduced as well in the lower levels to simulate multi-layer cloud regimes, so we can see what effect they would have on the retrievals of the ice-cloud properties here. These liquid clouds were placed near the surface and were prescribed optical depths of 1, 2, 5, 10, and 20. The effective diameter of these clouds was 20 microns, and they were placed about 1 kilometer above the surface. These clouds had the same thickness of 500 meters, and fall within the broad observed range of low-level cumulus observed at this site (Berg and Kassianov, 2008).

2.5 Information Content Calculation

To determine the sensitivity of each AIRS channel to changes in ice cloud properties, we use a scalar metric called Shannon information content (Shannon and Weaver, 1949). Shannon information content, described more in depth by Rodgers (2000), qualitatively can be defined as the factor by which knowledge of a quantity is improved by making a measurement. In other words, information content is the change in information provided following a measurement. This can be visualized in Figure 2.3 (L'Ecuyer et al., 2006). Here we see that when doing a retrieval of cloud properties, we start with the a priori knowledge of the scene we are measuring. As we incorporate radiance observations from different channels of our remote sensing instrument into our analysis, we can increase our certainty about the properties of the cloud present in the environment. This decrease in uncertainty is quantified in the metric known as information content. As we continue to incorporate more measurements from different spectral channels, we can further decrease

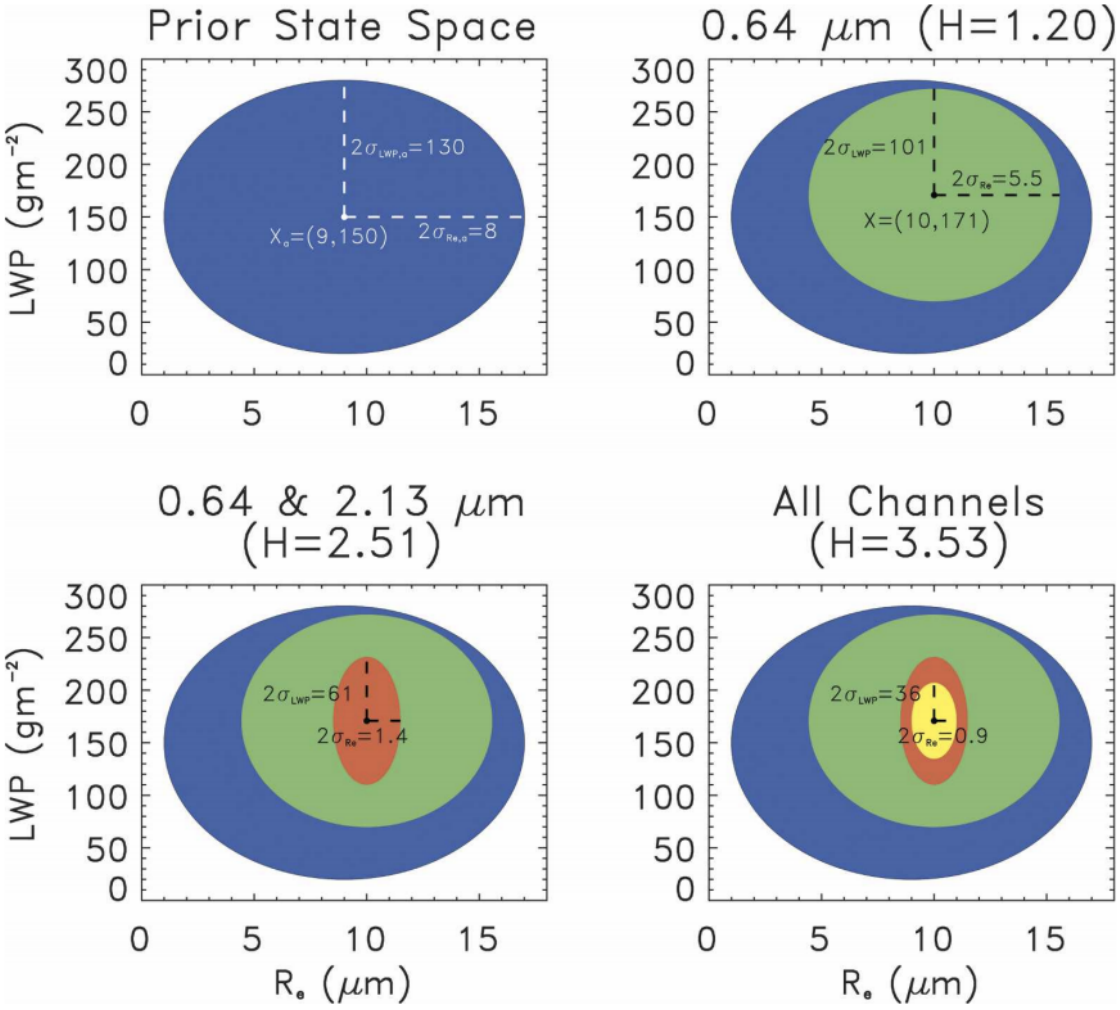

FIGURE 2.3: Graphical representation of the impact of adding information in a two-dimensional retrieval using the retrieval of effective radius and liquid water path (LWP) from shortwave reflectance measurements as an example. Each ellipse represents the projection of the corresponding two-dimensional posterior Gaussian probability density function of solutions at the level that encompasses 95% of the possible solutions (L'Ecuyer et al., 2006)

our uncertainty behind the cloud properties we are trying to retrieve, until eventually we have a more accurate estimate of the cloud properties of the observed clouds in the scene. The first measurement we incorporate into our retrieval contains the most information, and continual measurements will further decrease the uncertainty with a retrieval until

additional measurements add little additional information to what we know already about the clouds we are observing.

To calculate information content, we will be following the steps outlined in Rodgers (2000). We start with the a priori knowledge about the cloud properties we are observing. The probability density function (PDF) of variables in a dataset is used as a measure of the information of a system, or a system's entropy S, where p_i is the probability of the system being in state i. Here, a system's entropy can be defined as the change in the logarithm of the number of distinct possible internal states of the system being measured:

$$S(P) = -\Sigma p_i ln(p_i) \tag{2.1}$$

This means that information content H, which is the change in information following a measurement, can be written as follows. Here, P_1 describes the knowledge before a measurement and P_2 describes the knowledge after a measurement:

$$H = S(P_1) - S(P_2) \tag{2.2}$$

In other words, Shannon information content describes the decrease in uncertainty of a system state following a measurement.

We can apply this methodology to remote sensing, where the measurements here are from the AIRS channels and the variables of interest are the cloud variables from the prior clustering database. Here, we assume a linear Gaussian distribution for the prior and posterior PDFs, as done in Rodgers (2000). We can then rewrite our equation for

the information content of each AIRS channel, H, as follows,

$$H = S\left[P\left(x\right)\right] - S\left[P\left(x|y\right)\right] \tag{2.3}$$

$$= \frac{1}{2} ln|\mathbf{S_a}| \; - \; \frac{1}{2} ln|\hat{\mathbf{S}}| \tag{2.4}$$

$$= \frac{1}{2} ln|\hat{\mathbf{S}}^{-\mathbf{1}}\mathbf{S_a}| \tag{2.5}$$

where $\mathbf{S_a}$ and $\hat{\mathbf{S}}$ are the prior and posterior error covariance of the retrieved variables, respectively. Here, $\mathbf{S_a}$ is obtained from the climatological variance of the natural log of the retrieved cloud properties (ice cloud optical depth, effective diameter [μm], and cloud top temperature [K]) from the ARM SGP ice cloud data set that we compiled. $\mathbf{S_a}$ is a 3x3 matrix populated by the variance of the ice cloud properties in its diagonal, and the covariance of these properties in its off-diagonal elements, listed below:

$$\mathbf{S_a} \; = \; \begin{bmatrix} \underset{4.927}{\text{var } [\ln(\tau)]} & \underset{0.655}{\text{cov } [\ln(\tau),\ \ln(\mathrm{D_e})]} & \underset{-0.014}{\text{cov } [\ln(\tau),\ \ln(\mathrm{CTT})]} \\ \underset{0.655}{\text{cov } [\ln(\tau),\ \ln(\mathrm{D_e})]} & \underset{0.277}{\text{var } [\ln(\mathrm{D_e})]} & \underset{0.011}{\text{cov } [\ln(\tau),\ \ln(\mathrm{D_e})]} \\ \underset{-0.014}{\text{cov } [\ln(\tau),\ \ln(\mathrm{CTT})]} & \underset{0.011}{\text{cov } [\ln(\mathrm{D_e}),\ \ln(\mathrm{CTT})]} & \underset{0.002}{\text{var } [\ln(\mathrm{CTT})\ ]} \end{bmatrix}$$

$\hat{\mathbf{S}}^{-\mathbf{1}}$ can be written as the following, as shown in Rodgers (2000):

$$\hat{\mathbf{S}}^{-\mathbf{1}} \; = \; \mathbf{K^T} {\mathbf{S}_\epsilon}^{-\mathbf{1}} \mathbf{K} \; + \; \mathbf{S_a^{-1}} \tag{2.6}$$

Here, $\mathbf{K}$ is the calculated Jacobian matrix. The Jacobian matrix contains the first-order partial derivatives of the simulated radiances at each AIRS channel with respect to various ice cloud parameters. In other words, it represents the sensitivity of the radiances simulated at each AIRS channel to the ice cloud parameters, specifically ice cloud optical depth, effective diameter, and cloud top temperature. We define the Jacobian matrix $\mathbf{K}$ as

$$\mathbf{K} = \begin{bmatrix} \frac{\partial I_{\upsilon_1}}{\partial ln(\tau)} & \frac{\partial I_{\upsilon_1}}{\partial ln(D_e)} & \frac{\partial I_{\upsilon_1}}{\partial ln(CTT)} \\ \frac{\partial I_{\upsilon_2}}{\partial ln(\tau)} & \frac{\partial I_{\upsilon_2}}{\partial ln(D_e)} & \frac{\partial I_{\upsilon_2}}{\partial ln(CTT)} \\ \vdots & \vdots & \vdots \\ \frac{\partial I_{\upsilon_N}}{\partial ln(\tau)} & \frac{\partial I_{\upsilon_N}}{\partial ln(D_e)} & \frac{\partial I_{\upsilon_N}}{\partial ln(CTT)} \end{bmatrix}$$

where I_{υ_i} is the radiance of channel i at AIRS channel υ_i, τ is cloud optical depth, D_e is effective diameter, and CTT is cloud top temperature. Each row represents how sensitive the radiances simulated at each channel are to incremental changes in ice cloud properties. $\mathbf{S}_\epsilon$ is the measurement error covariance matrix, defined as the sum of individual, uncorrelated error covariance matrices from the various measurement sources of error,

$$\mathbf{S}_\epsilon = \mathbf{S_y} + \mathbf{S_T} + \mathbf{S_{wv}} + \mathbf{S_{habit}} + \mathbf{S_{aerosol}} \tag{2.7}$$

where $\mathbf{S_y}$ is the instrument error covariance matrix which is assumed to be diagonal, $\mathbf{S_T}$ is the temperature uncertainty, $\mathbf{S_w v}$ is the humidity uncertainty, $\mathbf{S_{habit}}$ is the error due to ice crystal assumptions, and $\mathbf{S_{aerosol}}$ is the error due to aerosols. Here, $\mathbf{S}_\epsilon$ is a non-diagonal matrix; however, when calculating the information content of each channel, only

the diagonal elements are used, as we will see below. The AIRS instrument error matrix, $\mathbf{S_y}$, is derived using the AIRS NeDT (Noise Equivalent Temperature Difference) values, and the other relative values for the various sources of uncertainty used to calculate the error covariance matrix $\mathbf{S}_\epsilon$ are shown in Figure 2.4. The methods used to calculate these various measurement sources of error are derived from Chang et al. (2017), and will not be discussed in-depth here.

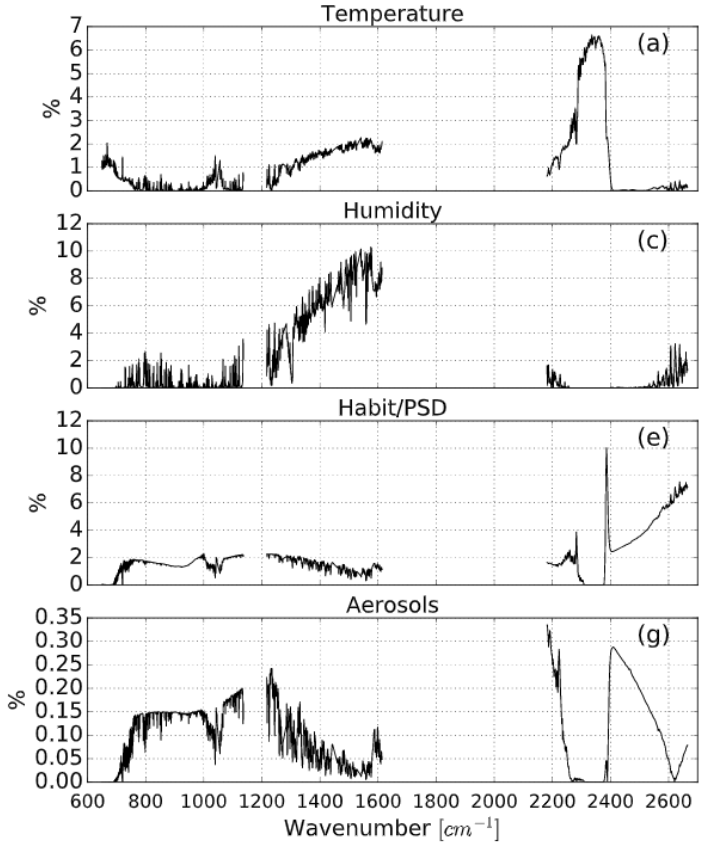

FIGURE 2.4: Uncertainty due to the specified source for AIRS channels. Percentages indicate the magnitude of the error standard deviation relative to the mean radiance of the simulations used to generate each uncertainty (Chang et al., 2017)

The error estimates associated with each channel from the various measurement uncertainties are incorporated into the calculation of information content for each channel;

if one channel has high errors associated with one of the measurement sources above, for instance due to instrument error, the information content contained in that channel might be less than other channels. The measurement of that channel has a high uncertainty associated with it; thus, adding it to our analysis would not necessarily decrease our uncertainty about the cloud properties being observed.

Using this methodology, we are able to calculate the information content of each AIRS channel observation based on each channel's sensitivity to ice cloud optical depth, effective diameter, and cloud top temperature, while incorporating various sources of uncertainty into the calculation. We modify the equations above so that we can calculate the information content of each channel H_i as follows:

$$H \;=\; \frac{1}{2}\, ln\, |\mathbf{S_a}\, (\mathbf{K^T S_\epsilon}^{-1} \mathbf{K} \;+\; \mathbf{S_a^{-1}})| \tag{2.8}$$

$$H_i \;=\; \frac{1}{2}\, ln\, |\mathbf{S_a}\, (\mathbf{k_i^T} \sigma_i^{-2}\, \mathbf{k_i} \;+\; \mathbf{S_a^{-1}})| \tag{2.9}$$

Here, σ_i^{-2} represents the diagonal element of $\mathbf{S_\epsilon}^{-1}$ for channel i.

After the information content is calculated for all channels, the channel with the most information is selected. Since we want to incorporate multiple AIRS channels into our analysis to maximize the information we gain about the ice clouds, we select the channel with the most information first, remove it from consideration, and repeat the selection process again. The selected channel is then "added" to the a priori error covariance

matrix $\mathbf{S_a}$ in the following manner,

$$\mathbf{S_{a,\ new}} = (\mathbf{k_i^T}\ \sigma_i^{-2}\ \mathbf{k_i}\ +\ \mathbf{S_a^{-1}})^{-1} \tag{2.10}$$

where k_i is the i^{th} row of the Jacobian $\mathbf{K}$, and by assuming that the observation error covariance is diagonal, we get the error variance σ_i^{-2}. We then repeat the calculations and update the a priori error covariance matrix to select other channels that are most complimentary to those picked previously. We do this calculation three times, as done in Chang et al. (2017), to pick the top three channels that provide the most information about the cloud properties of interest.

An example of the product of these calculations is shown in Figure 2.5. Figure 2.5 shows the information content of each AIRS channel in the presence of one of the single-layer ice clouds we analyzed. Once we calculate the information content of each AIRS channel, we find the channel with the most information and add it to the a priori error covariance matrix, as described above, and repeat the process until we have our specified number of channels selected with the most information about the cloud scene. Notice how after each channel addition, the amount of information contained in each channel measurement decreases. This occurs because our uncertainty about the cloud properties we wish to retrieve is decreasing, and so there is not as more information to be gained as we incorporate more and more channels into our analysis.

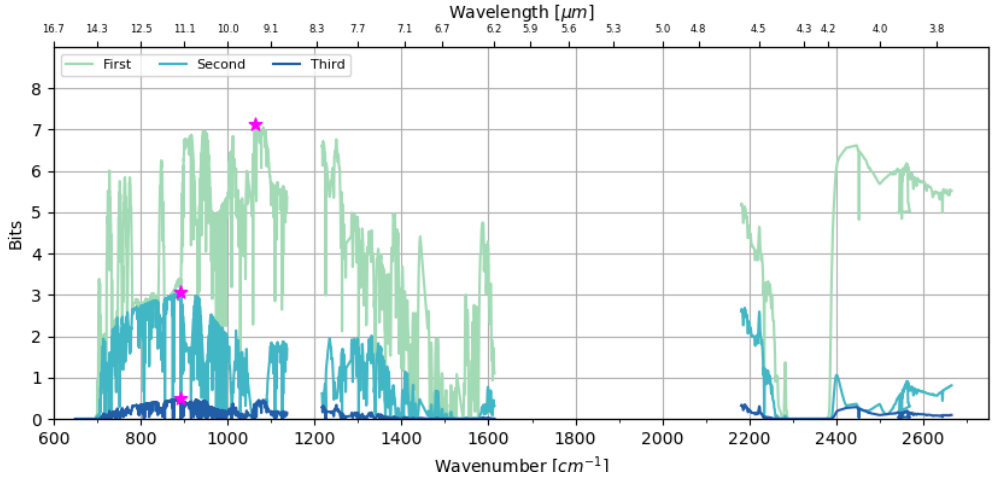

FIGURE 2.5: Example of calculated values of information content for all channels in the AIRS spectrum. This example is for one of the single-layer ice cloud clusters we analyzed. The channels with the most information content after each of the three iterations are starred.

Chapter 3

Results

From our initial results, we can see that there are some noticeable differences in atmospheric radiances in cases with single-layer ice clouds and multi-layer clouds. Figure 3.1 shows an example of one of the ice cloud clusters that was analyzed, with the modeled AIRS brightness temperature spectra plotted for the single-layer cloud and the five multi-layered cases that involve that upper-level ice cloud. We see immediately that once a low cloud is introduced beneath the upper-level ice cloud, the observed brightness temperatures from AIRS change noticeably in the shorter wavelength part of the AIRS spectrum (3.8-4.2 μm) and in the broad infrared window region (8-13 μm). In fact, the brightness temperatures in the shorter wavelengths increases as we transition to multi-layer scenes, whereas brightness temperatures decrease in the window region as we transition to multi-layer scenes. This makes sense, as in multi-layer cloud scenes, the presence of an optically

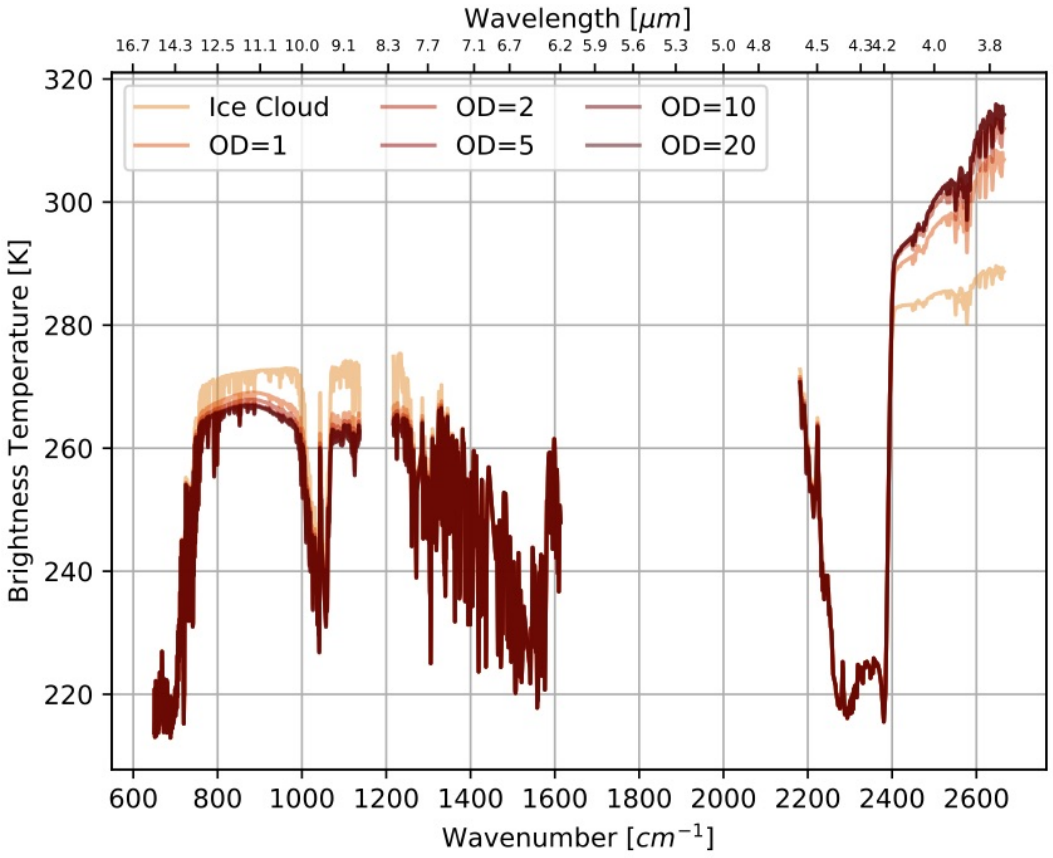

FIGURE 3.1: An example of the brightness temperature spectra that we calculated for each ice cloud cluster using the radiative transfer model. This graph includes the spectra for the single-layer ice cloud ("Ice Cloud") as well as for the multi-layer scenes, with the same ice cloud cluster as the single-layer case, but with an additional low-level cloud with varying optical depths (1, 2, 5, 10, and 20).

thick low cloud can increase the reflection of radiation at the shorter wavelengths, increasing observed brightness temperatures. Furthermore, in multi-layer scenes, the presence of low-level clouds, when compared to the surface, reduces the outgoing longwave radiation from the surface reaching the top of the atmosphere; this explains the decrease in the observed brightness temperature in the infrared window region in the multi-layer cloud scenes compared to single-layer scenes. In essence, the presence of the lower-level cloud is

creating a more reflective, cooler surface above which the upper-level ice clouds sit; thus, we see increased reflection in the shorter wavelengths as well as decreased emission in the longer wavelengths in these multi-layer scenes.

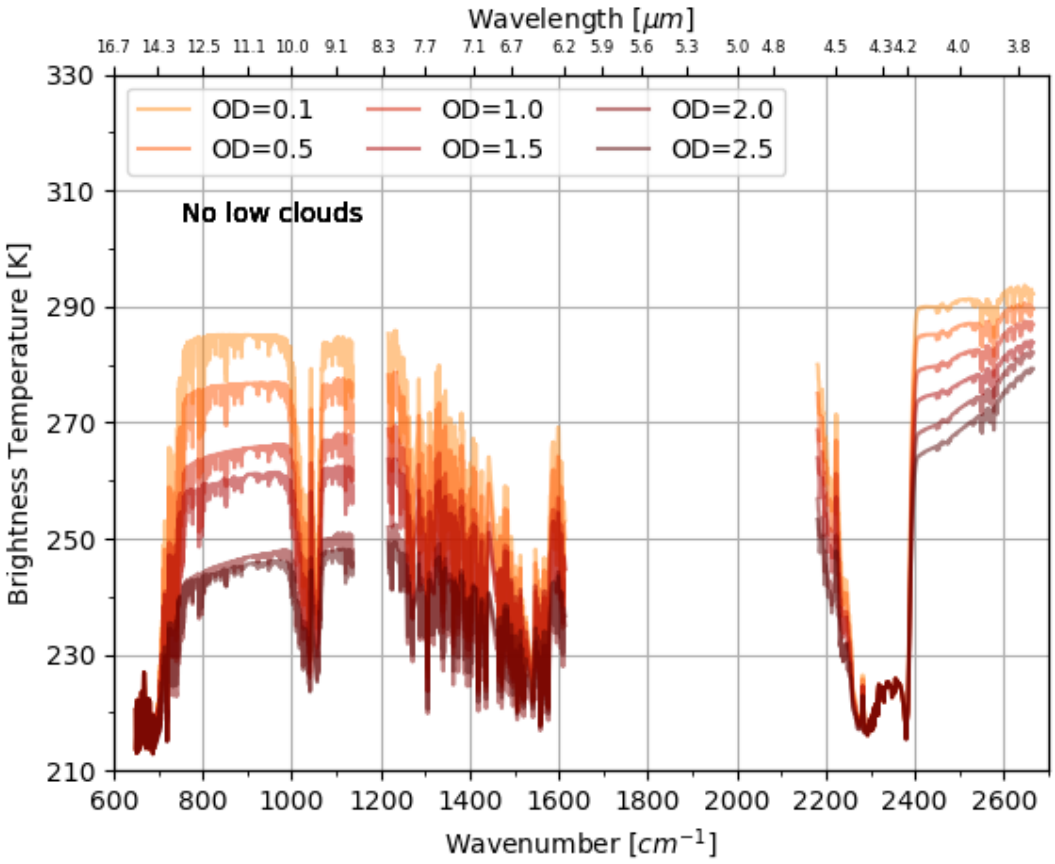

FIGURE 3.2: An example of brightness temperature spectra showing the effect that increasing the ice cloud optical depth of single-layer ice clouds has on the observed brightness temperatures. The plotted brightness temperature spectra are from ice cloud clusters with varying optical depths; their height and particle size, however, are not consistent, so effects of differing particle size and altitude may influence the spectra.

When we analyze the brightness temperature for various single-layer ice clouds Figure 3.2, we can see the effects of increasing optical depth of our single-layer ice clouds on the observed brightness temperatures. While particle size and cloud top temperature

of these clouds are not constant, we can still get meaningful qualitative insights into the sensitivity of various AIRS channels to the various ice cloud properties. We see that AIRS channels in the broad infrared window region (from 8-13 μm) seem to be the most sensitive to the optical depth of our ice clouds, as the brightness temperatures in this region are separating as the optical depth of our single-layer ice clouds change. This occurs in the shortwave region of the spectrum as well to a lesser extent.

When we look at multi-layer clouds, we see similar but slightly different sensitivities in these two spectral regions. Figure 3.3 shows an example of brightness temperatures modeled among various multi-level cloud scenarios. Here, the low-level cloud is the same, but the upper-level ice cloud is increasing in optical depth, and again, the cloud top temperature and particle size of the upper-level ice clouds are not held constant. We see here that with the presence of a low cloud, the shortwave region between 3.8 and 4.2 μm is even more sensitive than the single-layer cases to changes in upper-level ice cloud optical depths. The separation between brightness temperatures increases even more than in the single-layer cases, indicating that these shorter wavelengths might be useful for retrievals of upper-level ice cloud properties in multi-layer scenes. The infrared window region is also still sensitive to the ice cloud optical depths, although to a lesser extent than the single-layer cases, indicating that channels in this range may not contain as much information about the ice cloud properties as the shorter wavelengths in the AIRS spectrum in multi-layer cloud scenarios. This qualitative analysis here is a good overview to the information content analysis we are conducting, and allows us to have a more physical interpretation of the information content calculations that follow.

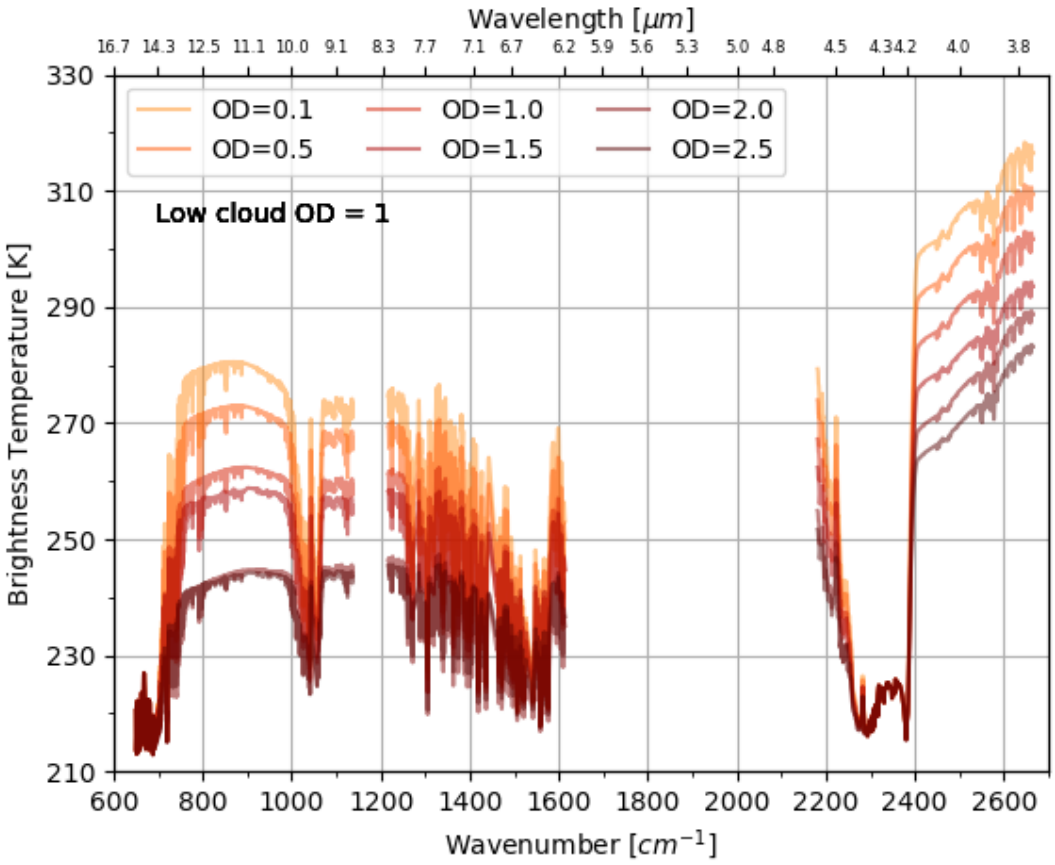

FIGURE 3.3: An example of brightness temperature spectra showing the effect that increasing the ice cloud optical depth of ice clouds in multi-layer cloud scenes has on observed brightness temperatures. The plotted brightness temperature spectra are from ice cloud clusters with varying optical depths, with a low-level liquid cloud that has an optical depth of 1 beneath them. The height and particle size of the ice clouds are not consistent, so effects of differing particle size and altitude may influence the spectra.

Figure 3.4 shows the results of the information content calculations and channel selections for each simulated single-layer ice cloud scenario. For single-layer ice clouds, we find that the channels that are selected most frequently overall fall near 1050 cm^{-1} (9.5 μm) and between 850-950 cm^{-1} (10.5-11.8 μm), although channels near 1050 cm^{-1} (9.5 μm) were selected first most frequently, and thus contained the most information

overall in these single-layer ice cloud scenarios. Other peaks in channel selection, in order of selection frequency, occurred near 1000 cm^{-1} (10 μm), 725-825 cm^{-1} (12.1-13.8 μm), 2175 cm^{-1} (4.6 μm), 1200-1250 cm^{-1} (8 - 8.3 μm), and 2625 cm^{-1} (3.8 μm).

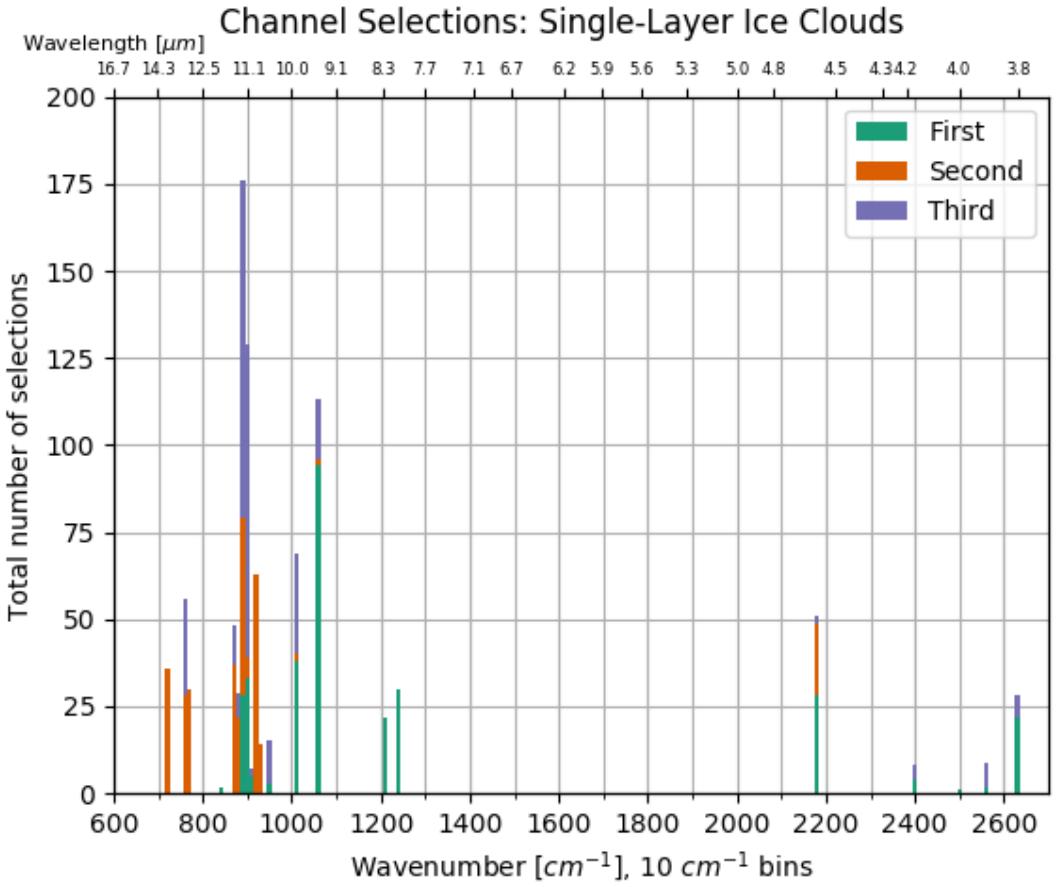

FIGURE 3.4: The channels that had the most information about single-layer ice clouds for all of the ice clusters analyzed with both grass and ocean ground surfaces. The selections are grouped into 10 cm^{-1} bins, and they are colored by the order that they were selected (see Figure 2.5).

Overall, the channels selected most frequently fell in the broad infrared window region of the AIRS spectrum (8-13 μm), which is what we predicted from qualitatively comparing brightness temperatures for single-layer ice clouds of varying optical depths. While some channels in the shortwave part of the AIRS spectrum are selected as containing the most

information about single-layer ice clouds, these channels were selected infrequently, if at all. These shorter wavelength channels overall seemed to contain much less information than those found in the longer wavelength part of the AIRS spectrum.

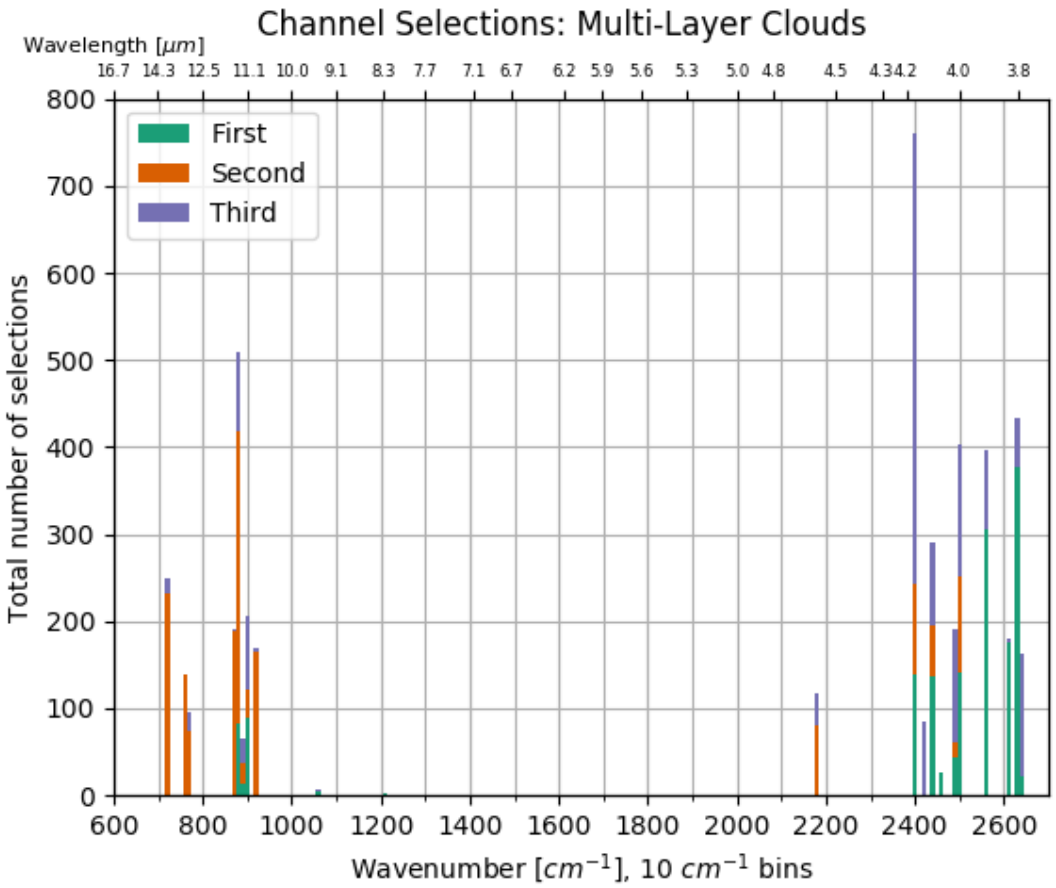

FIGURE 3.5: The AIRS channels that had the most information about ice clouds in multi-layer scenes. This includes the results for all of the ice clusters analyzed, each grouped with five different low-level liquid clouds of varying optical depth, with both grass and ocean ground surfaces. The selections are grouped into 10 cm^{-1} bins, and they are colored by the order that they were selected (see Figure 2.5).

However, once lower-level liquid clouds were introduced, the channels with the most information content about the ice cloud properties changed. Figure 3.5 shows the

results of the information content calculations and channel selections for each simulated multi-layer cloud scenario. This includes all simulations of the 156 ice cloud clusters, each above the five different low-level clouds we introduced with varying optical depths. The channels selected most frequently in these multi-layer scenes shifted to the shortwave part of the spectrum, and are primarily concentrated between 2400-2650 cm^{-1} (3.8-4.2 μm). These channels, which were rarely selected as containing the most information in single-layer cases, became significantly more important once a low-level cloud was introduced into the column. Channel selections between 850-950 cm^{-1} (10.5-11.8 μm) still were selected frequently in the multi-layer scenes, as well as channels between 725-825 cm^{-1} (12.1-13.8 μm) and 2175 cm^{-1} (4.6 μm). However, the shortwave channels were selected with much higher frequency in the multi-layer scenes.

Figure 3.6 summarizes the results we found from our information content analysis. Figure 3.6a shows the channels with the most information for the single-layer ice cloud cases, while Figure 3.6b-f shows the channels with the most information about ice clouds in the multi-layer cases, with optical depth of the low cloud increasing down the y-axis. We can see that in multi-layer cases, as the low-level cloud's optical depth increased, shorter wavelength channels were selected more frequently than the longer wavelength channels overall as containing the most information about ice cloud properties. This shift is just a shift in the frequency of channel selection. New channels or ranges of channels were not being selected with different low-level clouds; rather, the same channels were selected in nearly all of our multi-layer cloud scenarios, but the frequency of selection is what changed, with the shortwave channels being selected more frequently as the optical

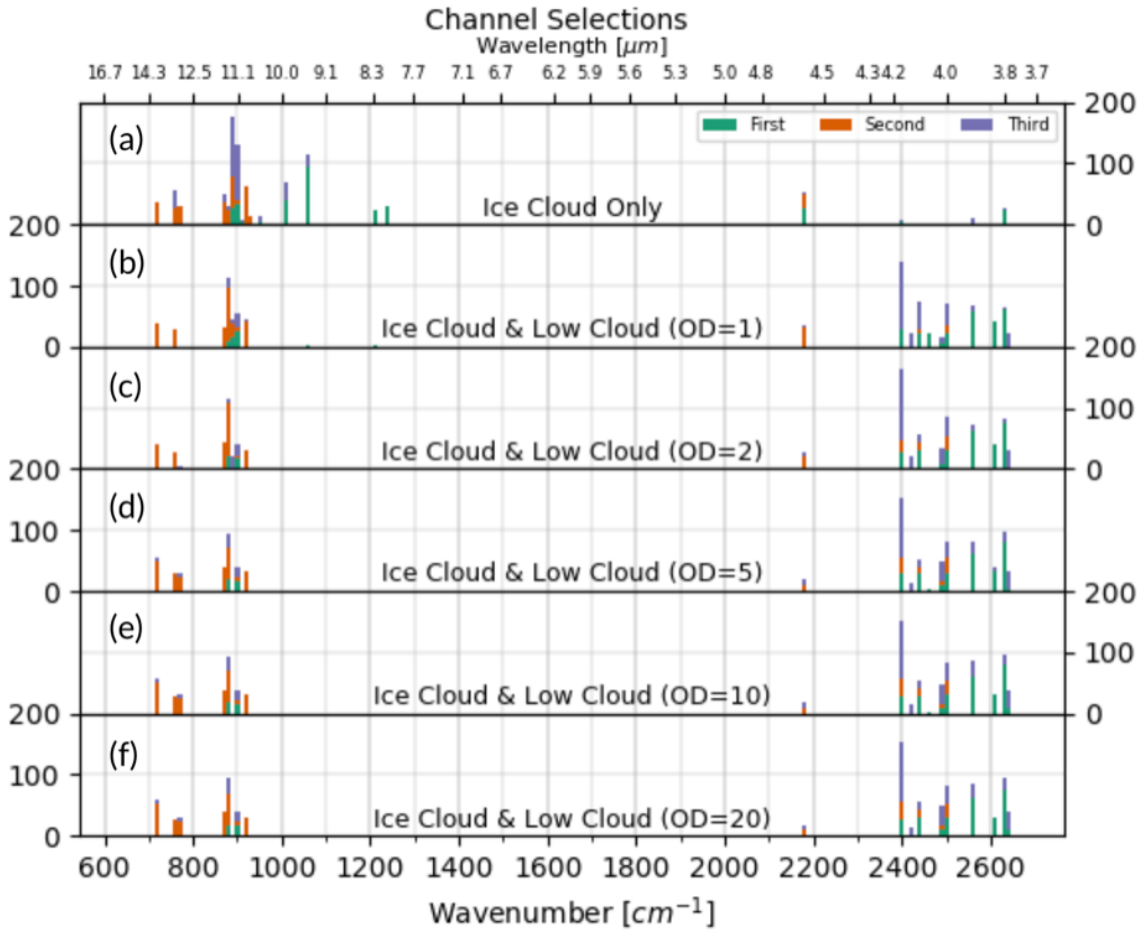

FIGURE 3.6: (a) AIRS channels with the most information about ice clouds for the single-layer cases, grouped into 10 cm^{-1} bins. (b) AIRS channels with the most information about ice clouds for the multi-layer cases, with all ice-cloud clusters above a standard low cloud, with an optical depth of 1, grouped into 10 cm^{-1} bins. (c) Same as (b), but the low cloud has an optical depth of 2. (d) Same as (b), but the low cloud has an optical depth of 5. (e) Same as (b), but the low cloud has an optical depth of 10. (f) Same as (b), but the low cloud has an optical depth of 20.

depth of the lower-level cloud increased. However, this effect saturates with increasing low-level optical depth, to the point where after the low-level cloud's optical depth exceeds a value of 5, the channels selected seem to remain the same as the low-level cloud becomes more optically thick. An example of this saturation effect is pictured in Figure 3.7; here, the channels selected transition from longer wavelengths to shorter wavelengths as the

optical depth of the low cloud increases. While most scenarios transition to short wavelength selections as soon as low clouds are introduced, some transition as the low cloud's optical depth begins to increase. Furthermore, what is interesting about this result is that the amount of information about the upper-level ice cloud tends to increase, specifically in the shortwave spectrum, once the scene transitions from a single-layer ice cloud scene to a multi-layer scene. From this analysis, we can start to see that the amount of information available in the AIRS shortwave channels about the upper-level ice clouds is higher in multi-layer cloud scenes than single-layer scenes; however, this claim needs to be tested more robustly to be definitive, and theories for why this is need to be explored.

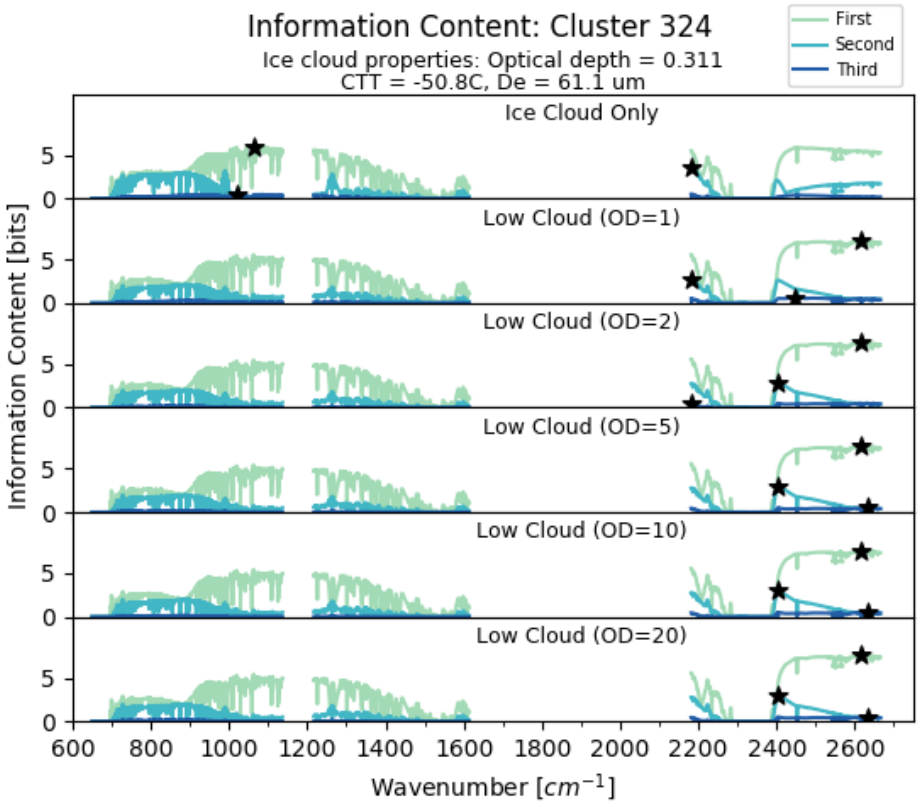

FIGURE 3.7: An example of the information content calculation and channel selection (see Figure 2.5) for the single-layer case (top) and the multi-layer cases.

Chapter 4

Discussion

The channels selected here for the retrieval of ice clouds in single- and multi-layer scenes fall in line with many cloud-retrieval analyses and algorithms. Channels in the infrared window region were often selected to contain high values of information about ice clouds for both single- and multi-layer cases. This makes sense, as the absence of absorption by atmospheric constituents allows for easier retrievals of cloud top temperature. Specifically, the split-window technique, which utilizes differences in brightness temperatures between two channels near 10.8 and 12 μm, has been shown to be successful at retrieving the properties of thin cirrus, specifically related to optical depth and particle size (Inoue 1985; Prabhakara et al. 1988). Channels selected in the longer part of the AIRS spectrum, specifically near 725-825 cm^{-1} (12.1-13.8 μm), fall near the CO_2 absorption band, and are utilized in the CO_2 slicing technique to retrieve the vertical position of clouds, especially for optically thin clouds like cirrus (Smith and Platt 1978; Minnis 2002).

For multi-layer clouds, we saw that channels in the shortwave part of the AIRS spectrum, specifically from 2400-2650 cm^{-1} (3.8-4.2 μm), contained a significant amount of information about the upper-level ice clouds. The source of radiation in this shortwave range is almost certainly from sunlight being reflected off of low-level clouds. Higher observed radiances in this shortwave window region near 4 μm, compared to in the 11 μm infrared window region, can distinguish clouds from the ground and can indicate that there is indeed a low-level cloud present or that multiple cloud layers exist in the column (Minnis, 2002). Therefore, coupling measurements in the shortwave and infrared window regions can distinguish single-layer from multi-layer cloud regimes, similar to what we saw in our information content analysis of multi-layer cloud scenes. However, these joint measurements go beyond simply identifying multi-layer cloud scenes; rather, these joint shortwave and longwave measurements have been further utilized to retrieve cloud properties as well, including particle size and other optical properties (Arking and Childs 1985; Minnis 2002; Stephens and Kummerow 2007). One caveat of using these shortwave channels, however, is that the source of radiation in the shortwave channels is primarily from the sun; thus, these channels might not be as useful at night, and separate retrievals may need to account for diurnal changes in the observed radiances in the shortwave spectrum.

While the methodology behind these current retrieval methods is different than what is used in this information content analysis, seeing that similar wavelength channels have been used before for retrievals of ice cloud properties confirms that the channels we have selected contain information about the properties of ice clouds in both single- and

multi-layer scenes. Thus, using the results of our information content analysis to create a retrieval algorithm for the properties of ice clouds in single- and multi-layer scenes seems promising, a step we hope to take in the future.

Chapter 5

Conclusion

5.1 Summary of findings

Our quest to find the optimal set of channels that can be used to retrieve the properties of ice clouds in single- and multi-layer scenes has left us with promising results. In both single- and multi-layer cloud scenes, we find that AIRS channels near 11 μm, 13-14 μm, and 4.6 μm contain information about the properties of observed ice clouds. However, in single-layer cases, channels near 8 μm, and from 9.5 – 10 μm contained information about the single-layer ice clouds, but did not provide information about ice clouds in multi-layer scenes. In multi-layer cases, channels from 3.8-4.2 μm contained information about ice clouds, whereas in single-layer environments these channels were rarely selected as containing the most information about ice clouds. Thus, we have found that a one-size-fits-all approach to retrieving ice cloud properties might not necessarily be useful

when creating retrieval algorithms, as channels with information about ice clouds are sensitive to the presence of underlying liquid clouds. Thus, improving techniques to test for the presence or absence of low-level clouds in the presence of upper-level ice clouds is essential to improving the retrieval of ice-cloud properties in the mid-latitudes and on a global scale.

Our results have some limitations, based on the assumptions we made and the dataset used in this analysis. In terms of assumptions made with the radiative transfer model, our analysis assumed daytime conditions, 100% overcast conditions, a standardized atmospheric profile, and we assumed measurement noise based on a variety of estimates. The cloud dataset used to create the ice-cloud clusters we analyzed was derived from the ARM Southern Great Plains site, using five basic low-level clouds to simulate multi-layer cloud scenes. While our assumptions attempted to create idealized mid-latitude scenes with realistic measurement error estimates, these assumptions may not be applicable in all cloud scenes or in more unique sub-regions within the mid-latitudes, and our results may be sensitive to our assumptions about various sources of error. These assumptions indicate that our results for these theoretical scenes might not be applicable for all observed single- and multi-layer cloud scenes, and further sensitivity analyses would improve our confidence in these results.

5.2 Future work

Expanding our information content analysis to include other passive instruments onboard the Aqua satellite, specifically MODIS, could improve retrievals of cirrus cloud properties.

MODIS operates similarly to AIRS, but contains more channels in the shortwave spectrum, which as we see from our results, contain information about the properties of ice clouds in multi-layer cloud scenes. This joint information content analysis of MODIS and AIRS instruments has been done before (Chang et al., 2017), and combining measurements from these two collocated instruments can add additional information to retrievals of ice clouds.

Expanding the number of ice cloud clusters and liquid clouds that we analyze could enhance the robustness of our results and enhance our understanding of the reasons why some channels are selected more frequently than others. One of the ways we can do that is analyzing more of the cloud clusters not initially selected in this analysis, such as those with larger optical depths that may have had too large of an effective diameter or too large of a spread in cloud optical depth to include in our current analysis. The ice-cloud clusters we analyzed all had optical depths below 10; while our goal was to analyze optically thin ice clouds, expanding our analysis to optically thicker clouds will improve our understanding of channel selections for a variety of upper-level ice clouds and make our results more robust. Similarly, incorporating ice clouds over ocean surfaces could increase our confidence in our results as well. In our analysis, we created generalized ice cloud clusters that were derived from measurements of ice clouds over the ARM SGP site. While our results are meant to be general, and the ice clusters we analyzed encapsulate a broad array of observed ice cloud types, the results are based on a cloud dataset observed over land. Upper-level ice clouds over land may contain some inherent differences to those observed over ocean due to the dominant formation mechanisms or

synoptic-scale conditions, and finding a way to incorporate oceanic ice clouds into our analysis could make our results more robust. Similarly, in this study, to simulate multi-layered clouds, we incorporated idealized low-level clouds of various optical depths into the vertical profiles; these low-level clouds were not based on observations. One way to improve our simulations of multi-layer clouds is to use observations of low-level liquid clouds, like we did with the ice clouds in this analysis, rather than prescribed low-level clouds, in order to fully encapsulate the variation in multi-layer cloud regimes. If we were to do this, incorporating observed low-level liquid clouds over land and ocean would be beneficial as well, as the low-level liquid clouds over land and ocean can be inherently different from each other based on their varying formation mechanisms.

Analyzing the effect of our background atmospheric profile, our radiative transfer model assumptions, and our sources of error on our results could increase our confidence in our results as well. Varying the background atmospheric profile used in this analysis could simulate more mid-latitude atmospheric regimes, as the generalized background profile we used might not always be representative of the scene on hand. Varying the atmospheric profile could confirm that the results we see are not a strong function of trace gases, specifically ozone, carbon monoxide, methane, and carbon dioxide. Furthermore, pre-excluding channels in strong gaseous absorption bands, and comparing the results to what we derived here, would be an interesting analysis. We also assume daytime conditions in the forward model calculations. Thus, we need to take this into account when using our results in an operational ice cloud retrieval. During daytime conditions,

complications with solar contamination and non-LTE effects can cause the radiance measurements of shortwave infrared channels, specifically those above 2300 cm^{-1}, to be less reliable if they are not properly accounted for in the forward model. Thus, despite the information content that these channels may have, they might not be as reliable in an operational setting, and they might not be useful throughout the entire diurnal cycle. By varying the atmospheric profile to account for seasonal or regional differences, or finding a way to use real-time atmospheric data, we could improve our confidence that the AIRS channels selected as containing the most information are consistent throughout all mid-latitude sites and throughout the seasonal and diurnal cycles. Similarly, conducting an error sensitivity analysis could yield some interesting results. Modifying our assumptions about the various sources of error in our information content calculations, either by modifying individual sources of error or, say, by doubling our error estimates, for example, could help us see how robust our results are.

Conducting this analysis with a separate radiative transfer model could improve our confidence in our results. More specifically, using a radiative transfer model built to handle high-spectral-resolution channels, such as SARTA (Stand-alone AIRS Radiative Transfer Algorithm, Strow et al. 2003), which is specifically designed to simulate AIRS radiances, could reduce some of the uncertainty in our results. Finally, assumptions about the measurement noise may not always be appropriate for all mid-latitude scenes. Finding a more realistic error matrix, or perhaps finding a way to incorporate off-diagonal elements into the measurement error covariance matrix, needs further investigation before this approach could potentially be implemented in an operational setting. Looking

at the assumed error sources and analyzing the channels with the highest sources of error could yield some interesting insights into why some channels were selected over others.

With the current information we have from the model runs, we have an idea of which channels are most sensitive to changes in cloud optical depth, cloud top temperature, and cloud particle size. Breaking this analysis down, where we analyze the channel selections based on individual variables could provide insight into why certain channels are selected more frequently than others. By doing this, we could attribute channel selection to the cloud variables each channel is most sensitive to, and gain a deeper understanding of why certain channels are preferentially selected over others.

In this analysis, we have not developed a way to retrieve the cloud cluster properties given the radiances simulated by the radiative transfer model, and our results remain primarily theoretical. In theory, we should be able to take the radiances from the channels with the highest information content and create an algorithm to back out the cloud properties in the column that would be creating the modeled radiances. Operationally, the retrieval process might not be as easy. Challenges may arise due to the assumptions we have made in our methodology, which may not apply to all regional mid-latitude cloud scenes. Furthermore, challenges may arise from issues with instrumentation, with issues specific to the AIRS instrument that result from its grating instrument. For example, some AIRS channels have high noise due to dead or popping detectors, which make these channels unusable for retrievals (Pagano et al., 2012). Incorporating what we know about noisy channels and other instrumentation issues into our eventual retrieval method is essential for accurate retrievals. To avoid the issue of noisy channels altogether, we could

repeat this analysis with other advanced infrared sounders such as IASI or CrIS, which are Michelson Interferometers, both of which have some advantages over AIRS, including a continuous spectral coverage with over 8000 infrared channels on IASI or the lower noise on CrIS, as well as differences in instrumentation that allow these instruments to avoid popping sensors (Smith et al., 2015).

One method to retrieve the ice cloud properties from our results involves using optimal estimation (Rodgers, 2000), which has been used for a variety of cloud property retrievals previously. However, using other methods, such as Bayesian techniques, could improve our interpretation of our results and test the effectiveness of using information content for cloud property retrievals (Petty, 2018). Finally, confirming that the observations we are modeling are realistic can improve our confidence with our results. This can be done by looking at actual AIRS and MODIS measurements and comparing them to our simulations to make sure that the channels that have the most information in our theoretical analysis are useful in operational settings.

Bibliography

Ackerman, T. P. and G. M. Stokes, 2003: The Atmospheric Radiation Measurement Program. *Physics Today*, **56**, 38–44, doi:10.1063/1.1554135.

Anderson, G., S. Clough, and F. Kneizys, 1986: AFGL atmospheric constituent profiles. *Environ. Res. Pap.*, **954**, 1–46.

Arakawa, A., 1975: Modelling Clouds and Cloud Processes for Use in Climate Models. *The Physical Basis of Climate and Climate Modelling*, GARP Publications Series No. 16, WMO/ICSU, 183–197.

Arking, A. and J. D. Childs, 1985: Retrieval of Cloud Cover Parameters from Multispectral Satellite Images. *Journal of Climate and Applied Meteorology*, **24**, 322–333, doi:10.1175/1520-0450(1985)024¡0322:ROCCPF¿2.0.CO;2.

Baldridge, A., S. Hook, C. Grove, and G. Rivera, 2009: The ASTER spectral library version 2.0. *Remote Sensing of Environment*, **113**, 711–715, doi:10.1016/j.rse.2008.11.007.

Baum, B. A., P. Yang, A. J. Heymsfield, A. Bansemer, B. H. Cole, A. Merrelli, C. Schmitt, and C. Wang, 2014: Ice cloud single-scattering property models with the full phase

matrix at wavelengths from 0.2 to 100 μm. *Journal of Quantitative Spectroscopy and Radiative Transfer*, **146**, 123 – 139, doi:10.1016/j.jqsrt.2014.02.029.

Berg, L. K. and E. I. Kassianov, 2008: Temporal Variability of Fair-Weather Cumulus Statistics at the ACRF SGP Site. *Journal of Climate*, **21**, 3344–3358, doi:10.1175/2007JCLI2266.1.

Bodas-Salcedo, A., K. D. Williams, M. A. Ringer, I. Beau, J. N. S. Cole, J.-L. Dufresne, T. Koshiro, B. Stevens, Z. Wang, and T. Yokohata, 2014: Origins of the Solar Radiation Biases over the Southern Ocean in CFMIP2 Models. *Journal of Climate*, **27**, 41–56, doi:10.1175/JCLI-D-13-00169.1.

Bodhaine, B. A., N. B. Wood, E. G. Dutton, and J. R. Slusser, 1999: On Rayleigh Optical Depth Calculations. *Journal of Atmospheric and Oceanic Technology*, **16**, 1854–1861, doi:10.1175/1520-0426(1999)016¡1854:ORODC¿2.0.CO;2.

Boucher, O., D. Randall, P. Artaxo, C. Bretherton, G. Feingold, P. Forster, V.-M. Kerminen, Y. Kondo, H. Liao, U. Lohmann, P. Rasch, S. K. Satheesh, S. Sherwood, B. Stevens, and X. Y. Zhang, 2013: Clouds and Aerosols. *Climate Change 2013: The Physical Science Basis. Contribution of Working Group I to the Fifth Assessment Report of the Intergovernmental Panel on Climate Change*, T. Stocker, D. Qin, G.-K. Plattner, M. Tignor, S. K. Allen, J. Boschung, A. Nauels, Y. Xia, V. Bex, and P. M. Midgley, eds., Cambridge University Press, 571–658.

Chang, K.-W., T. S. L'Ecuyer, B. H. Kahn, and V. Natraj, 2017: Information content of visible and midinfrared radiances for retrieving tropical ice cloud properties. *Journal of Geophysical Research: Atmospheres*, **122**, 4944–4966, doi:10.1002/2016JD026357.

Eastman, R. and S. G. Warren, 2010: Interannual Variations of Arctic Cloud Types in Relation to Sea Ice. *Journal of Climate*, **23**, 4216–4232, doi:10.1175/2010JCLI3492.1.

Eliasson, S., S. A. Buehler, M. Milz, P. Eriksson, and V. O. John, 2011: Assessing observed and modelled spatial distributions of ice water path using satellite data. *Atmospheric Chemistry and Physics*, **11**, 375–391, doi:10.5194/acp-11-375-2011.

Hale, G. M. and M. R. Querry, 1973: Optical Constants of Water in the 200-nm to 200-μm Wavelength Region. *Appl. Opt.*, **12**, 555–563, doi:10.1364/AO.12.000555.

Hang, Y., T. S. L'Ecuyer, D. S. Henderson, A. V. Matus, and Z. Wang, 2019: Reassessing the Effect of Cloud Type on Earth's Energy Balance in the Age of Active Spaceborne Observations. Part II: Atmospheric Heating. *Journal of Climate*, **32**, 6219–6236, doi:10.1175/JCLI-D-18-0754.1.

Hartmann, D. L., V. Ramanathan, A. Berroir, and G. E. Hunt, 1986: Earth Radiation Budget data and climate research. *Reviews of Geophysics*, **24**, 439–468, doi:10.1029/RG024i002p00439.

Henderson, D. S., T. L'Ecuyer, G. Stephens, P. Partain, and M. Sekiguchi, 2013: A Multisensor Perspective on the Radiative Impacts of Clouds and Aerosols. *Journal of Applied Meteorology and Climatology*, **52**, 853–871, doi:10.1175/JAMC-D-12-025.1.

Inness, A., F. Baier, A. Benedetti, I. Bouarar, S. Chabrillat, H. Clark, C. Clerbaux, P. Coheur, R. J. Engelen, Q. Errera, J. Flemming, M. George, C. Granier, J. Hadji-Lazaro, V. Huijnen, D. Hurtmans, L. Jones, J. W. Kaiser, J. Kapsomenakis, K. Lefever, J. Leitão, M. Razinger, A. Richter, M. G. Schultz, A. J. Simmons, M. Suttie, O. Stein, J.-N. Thépaut, V. Thouret, M. Vrekoussis, C. Zerefos, and the MACC team, 2013: The MACC reanalysis: an 8 yr data set of atmospheric composition. *Atmospheric Chemistry and Physics*, **13**, 4073–4109, doi:10.5194/acp-13-4073-2013.

Inoue, T., 1985: On the Temperature and Effective Emissivity Determination of Semi-Transparent Cirrus Clouds by Bi-Spectral Measurements in the 10μm Window Region. *Journal of the Meteorological Society of Japan. Ser. II*, **63**, 88–99, doi:10.2151/jmsj1965.63.1_88.

Kahn, B. H., F. W. Irion, V. T. Dang, E. M. Manning, S. L. Nasiri, C. M. Naud, J. M. Blaisdell, M. M. Schreier, Q. Yue, K. W. Bowman, E. J. Fetzer, G. C. Hulley, K. N. Liou, D. Lubin, S. C. Ou, J. Susskind, Y. Takano, B. Tian, and J. R. Worden, 2014: The Atmospheric Infrared Sounder version 6 cloud products. *Atmospheric Chemistry and Physics*, **14**, 399–426, doi:10.5194/acp-14-399-2014.

Klein, S. A. and D. L. Hartmann, 1993: The Seasonal Cycle of Low Stratiform Clouds. *Journal of Climate*, **6**, 1587–1606, doi:10.1175/1520-0442(1993)006¡1587:TSCOLS¿2.0.CO;2.

L'Ecuyer, T. S. and J. H. Jiang, 2010: Touring the Atmosphere Aboard the A-Train. *Physics Today*, **63**, 36–41, doi:10.1063/1.3463626.

Lhermitte, R. M., 1988: Cloud and precipitation remote sensing at 94 GHz. *IEEE Transactions on Geoscience and Remote Sensing*, **26**, 207–216, doi:10.1109/36.3024.

Liou, K.-N., 1986: Influence of Cirrus Clouds on Weather and Climate Processes: A Global Perspective. *Monthly Weather Review*, **114**, 1167–1199, doi:10.1175/1520-0493(1986)114¡1167:IOCCOW¿2.0.CO;2.

Liu, C.-L. and A. J. Illingworth, 2000: Toward More Accurate Retrievals of Ice Water Content from Radar Measurements of Clouds. *Journal of Applied Meteorology*, **39**, 1130–1146, doi:10.1175/1520-0450(2000)039¡1130:TMAROI¿2.0.CO;2.

L'Ecuyer, T. S., P. Gabriel, K. Leesman, S. J. Cooper, and G. L. Stephens, 2006: Objective Assessment of the Information Content of Visible and Infrared Radiance Measurements for Cloud Microphysical Property Retrievals over the Global Oceans. Part I: Liquid Clouds. *Journal of Applied Meteorology and Climatology*, **45**, 20–41, doi:10.1175/JAM2326.1.

L'Ecuyer, T. S., Y. Hang, A. V. Matus, and Z. Wang, 2019: Reassessing the Effect of Cloud Type on Earth's Energy Balance in the Age of Active Spaceborne Observations. Part I: Top of Atmosphere and Surface. *Journal of Climate*, **32**, 6197–6217, doi:10.1175/JCLI-D-18-0753.1.

Mace, G. G., S. Benson, K. L. Sonntag, S. Kato, Q. Min, P. Minnis, C. H. Twohy, M. Poellot, X. Dong, C. Long, Q. Zhang, and D. R. Doelling, 2006: Cloud radiative

forcing at the Atmospheric Radiation Measurement Program Climate Research Facility: 1. Technique, validation, and comparison to satellite-derived diagnostic quantities. *Journal of Geophysical Research*, **111**, doi:10.1029/2005JD005921.

Mace, G. G., E. E. Clothiaux, and T. P. Ackerman, 2001: The Composite Characteristics of Cirrus Clouds: Bulk Properties Revealed by One Year of Continuous Cloud Radar Data. *Journal of Climate*, **14**, 2185–2203, doi:10.1175/1520-0442(2001)014¡2185:TCCOCC¿2.0.CO;2.

Mace, G. G. and F. J. Wrenn, 2013: Evaluation of the Hydrometeor Layers in the East and West Pacific within ISCCP Cloud-Top Pressure–Optical Depth Bins Using Merged CloudSat and CALIPSO Data. *Journal of Climate*, **26**, 9429–9444, doi:10.1175/JCLI-D-12-00207.1.

Mace, G. G., Q. Zhang, M. Vaughan, R. Marchand, G. Stephens, C. Trepte, and D. Winker, 2009: A description of hydrometeor layer occurrence statistics derived from the first year of merged CloudSat and CALIPSO data. *Journal of Geophysical Research: Atmospheres*, **114**, doi:10.1029/2007JD009755.

Marshall, J. and R. A. Plumb, 2007: *Atmosphere, Ocean, and Climate Dynamics*. Academic Press, 344 pp.

Minnis, P., 2002: Satellite Remote Sensing of Cirrus. *Cirrus*, Oxford University Press, 147–167.

NASA, 2003: Formation Flying: The Afternoon "A-Train" Satellite Constellation. The Earth Science Enterprise Series, 6.

Pagano, T. S., S. Broberg, H. H. Aumann, D. Elliott, E. Manning, and L. Strow, 2012: Performance status of the Atmospheric Infrared Sounder ten years after launch. *Proceedings of SPIE*, **8527**, doi:10.1117/12.977309.

Parkinson, C. L., A. Ward, and M. D. King, 2006: Earth science reference handbook: a guide to NASA's earth science program and earth observing satellite missions. *National Aeronautics and Space Administration*, 277.

Petty, G., 2006: *A First Course in Atmospheric Radiation*. Sundog Publishing, 459 pp.

Petty, G. W., 2018: On Some Shortcomings of Shannon Entropy as a Measure of Information Content in Indirect Measurements of Continuous Variables. *Journal of Atmospheric and Oceanic Technology*, **35**, 1011–1021, doi:10.1175/JTECH-D-17-0056.1.

Prabhakara, C., R. S. Fraser, G. Dalu, M.-L. C. Wu, R. J. Curran, and T. Styles, 1988: Thin Cirrus Clouds: Seasonal Distribution over Oceans Deduced from Nimbus-4 IRIS. *Journal of Applied Meteorology*, **27**, 379–399, doi:10.1175/1520-0450(1988)027¡0379:TCCSDO¿2.0.CO;2.

Ramanathan, V., R. D. Cess, E. F. Harrison, P. Minnis, B. R. Barkstrom, E. Ahmad, and D. Hartmann, 1989: Cloud-Radiative Forcing and Climate: Results from the Earth Radiation Budget Experiment. *Science*, **243**, 57–63, doi:10.1126/science.243.4887.57.

Rodgers, C. D., 2000: *Inverse Methods for Atmospheric Sounding*. World Scientific, 256 pp.

Rogers, R. and M. Yau, 1996: *A Short Course in Cloud Physics*. Butterworth-Heinemann, 304 pp.

Rothman, L., I. Gordon, A. Barbe, D. Benner, P. Bernath, M. Birk, V. Boudon, L. Brown, A. Campargue, J.-P. Champion, K. Chance, L. Coudert, V. Dana, V. Devi, S. Fally, J.-M. Flaud, R. Gamache, A. Goldman, D. Jacquemart, I. Kleiner, N. Lacome, W. Lafferty, J.-Y. Mandin, S. Massie, S. Mikhailenko, C. Miller, N. Moazzen-Ahmadi, O. Naumenko, A. Nikitin, J. Orphal, V. Perevalov, A. Perrin, A. Predoi-Cross, C. Rinsland, M. Rotger, M. Šimečková, M. Smith, K. Sung, S. Tashkun, J. Tennyson, R. Toth, A. Vandaele, and J. V. Auwera, 2009: The HITRAN 2008 molecular spectroscopic database. *Journal of Quantitative Spectroscopy and Radiative Transfer*, **110**, 533 – 572, doi:10.1016/j.jqsrt.2009.02.013.

Santer, B. D., R. Sausen, T. M. L. Wigley, J. S. Boyle, K. AchutaRao, C. Doutriaux, J. E. Hansen, G. A. Meehl, E. Roeckner, R. Ruedy, G. Schmidt, and K. E. Taylor, 2003: Behavior of tropopause height and atmospheric temperature in models, reanalyses, and observations: Decadal changes. *Journal of Geophysical Research*, **108**, doi:10.1029/2002JD002258.

Sassen, K., 2002: Cirrus Clouds: A Modern Perspective. *Cirrus*, Oxford University Press, 11–40.

Sassen, K. and J. R. Campbell, 2001: A Midlatitude Cirrus Cloud Climatology from the Facility for Atmospheric Remote Sensing. Part I: Macrophysical and Synoptic Properties. *Journal of the Atmospheric Sciences*, **58**, 481–496, doi:10.1175/1520-0469(2001)058¡0481:AMCCCF¿2.0.CO;2.

Sassen, K., Z. Wang, and D. Liu, 2008: Global distribution of cirrus clouds from CloudSat/Cloud-Aerosol Lidar and Infrared Pathfinder Satellite Observations (CALIPSO) measurements. *Journal of Geophysical Research*, **113**, doi:10.1029/2008JD009972.

Schneider, S. H., 1972: Cloudiness as a Global Climatic Feedback Mechanism: The Effects on the Radiation Balance and Surface Temperature of Variations in Cloudiness. *Journal of the Atmospheric Sciences*, **29**, 1413–1422, doi:10.1175/1520-0469(1972)029¡1413:CAAGCF¿2.0.CO;2.

Shannon, C. E. and W. Weaver, 1949: *The Mathematical Theory of Communication, Volume 1*. University of Illinois Press, 117 pp.

Sidran, M., 1981: Broadband reflectance and emissivity of specular and rough water surfaces. *Appl. Opt.*, **20**, 3176–3183, doi:10.1364/AO.20.003176.

Smith, N., W. L. Smith, E. Weisz, and H. E. Revercomb, 2015: AIRS, IASI, and CrIS Retrieval Records at Climate Scales: An Investigation into the Propagation of Systematic Uncertainty. *Journal of Applied Meteorology and Climatology*, **54**, 1465–1481, doi:10.1175/JAMC-D-14-0299.1.

Smith, W. L. and C. M. R. Platt, 1978: Comparison of Satellite-Deduced Cloud Heights with Indications from Radiosonde and Ground-Based Laser Measurements. *Journal of Applied Meteorology*, **17**, 1796–1802, doi:10.1175/1520-0450(1978)017¡1796:COSDCH¿2.0.CO;2.

Smith, W. L., E. Weisz, S. V. Kireev, D. K. Zhou, Z. Li, and E. E. Borbas, 2012: Dual-Regression Retrieval Algorithm for Real-Time Processing of Satellite Ultraspectral Radiances. *Journal of Applied Meteorology and Climatology*, **51**, 1455–1476, doi:10.1175/JAMC-D-11-0173.1.

Spurr, R. J., 2006: VLIDORT: A linearized pseudo-spherical vector discrete ordinate radiative transfer code for forward model and retrieval studies in multilayer multiple scattering media. *Journal of Quantitative Spectroscopy and Radiative Transfer*, **102**, 316 – 342, doi:10.1016/j.jqsrt.2006.05.005.

Stephens, G. L., 1978: Radiation Profiles in Extended Water Clouds. II: Parameterization Schemes. *Journal of the Atmospheric Sciences*, **35**, 2123–2132, doi:10.1175/1520-0469(1978)035¡2123:RPIEWC¿2.0.CO;2.

Stephens, G. L. and C. D. Kummerow, 2007: The Remote Sensing of Clouds and Precipitation from Space: A Review. *Journal of the Atmospheric Sciences*, **64**, 3742–3765, doi:10.1175/2006JAS2375.1.

Strow, L. L., S. E. Hannon, S. D. Souza-Machado, H. E. Motteler, and D. Tobin, 2003: An overview of the AIRS radiative transfer model. *IEEE Transactions on Geoscience and Remote Sensing*, **41**, 303–313, doi:10.1109/TGRS.2002.808244.

Stubenrauch, C. J., W. B. Rossow, S. Kinne, S. Ackerman, G. Cesana, H. Chepfer, L. Di Girolamo, B. Getzewich, A. Guignard, A. Heidinger, B. C. Maddux, W. P. Menzel, P. Minnis, C. Pearl, S. Platnick, C. Poulsen, J. Riedi, S. Sun-Mack, A. Walther, D. Winker, S. Zeng, and G. Zhao, 2013: Assessment of Global Cloud Datasets from Satellites: Project and Database Initiated by the GEWEX Radiation Panel. *Bulletin of the American Meteorological Society*, **94**, 1031–1049, doi:10.1175/BAMS-D-12-00117.1.

Wang, P. K., 2013: *Physics and Dynamics of Clouds and Precipitation*. Cambridge University Press, 467 pp.

Webster, P. J., 1994: The role of hydrological processes in ocean-atmosphere interactions. *Reviews of Geophysics*, **32**, 427–476, doi:10.1029/94RG01873.

Weisz, E., J. Li, W. P. Menzel, A. K. Heidinger, B. H. Kahn, and C.-Y. Liu, 2007: Comparison of AIRS, MODIS, CloudSat and CALIPSO cloud top height retrievals. *Geophysical Research Letters*, **34**, doi:10.1029/2007GL030676.

Weisz, E., W. L. Smith, J. Li, W. P. Menzel, and N. Smith, 2011: Improved Profile and Cloud Top Height Retrieval by Using Dual Regression on High-Spectral Resolution Measurements. *Imaging and Applied Optics*, doi:10.1364/HISE.2011.HWA4.

Wielicki, B. A. and L. Parker, 1992: On the determination of cloud cover from satellite sensors: The effect of sensor spatial resolution. *Journal of Geophysical Research*, **97**, 12799–12823, doi:10.1029/92JD01061.

Wilks, D., 2011: Cluster Analysis. *Statistical Methods in the Atmospheric Sciences*, Academic Press, volume 100 of *International Geophysics*, 603–616.

World Meteorological Organization, 2017: International Cloud Atlas: Definitions of Clouds. Accessed 27 August 2019, `https://cloudatlas.wmo.int/clouds-definitions.html`.

Zhang, M. H., W. Y. Lin, S. A. Klein, J. T. Bacmeister, S. Bony, R. T. Cederwall, A. D. Del Genio, J. J. Hack, N. G. Loeb, U. Lohmann, P. Minnis, I. Musat, R. Pincus, P. Stier, M. J. Suarez, M. J. Webb, J. B. Wu, S. C. Xie, M.-S. Yao, and J. H. Zhang, 2005: Comparing clouds and their seasonal variations in 10 atmospheric general circulation models with satellite measurements. *J. Geophys. Res.*, **110**, D15S02, doi:10.1029/2004JD005021.